JOURNAL OF GEOPHYSICAL RESEARCH, VOL. 103, NO. D7, PAGES 8401–8423, APRIL 20, 1998

Photochemistry in biomass burning plumes and implications for tropospheric ozone over the tropical South Atlantic

Denise L. Mauzerall,[1,2] Jennifer A. Logan,[1] Daniel J. Jacob,[1] Bruce E. Anderson,[3] Donald R. Blake,[4] John D. Bradshaw,[5] Brian Heikes,[6] Glenn W. Sachse,[3] Hanwant Singh,[7] and Bob Talbot[8]

Abstract. Photochemistry occuring in biomass burning plumes over the tropical south Atlantic is analyzed using data collected during the Transport and Atmospheric Chemistry Near the Equator-Atlantic aircraft expedition conducted during the tropical dry season in September 1992 and a photochemical point model. Enhancement ratios ($\Delta Y/\Delta X$, where Δ indicates the enhancement of a compound in the plume above the local background mixing ratio, Y are individual hydrocarbons, CO, O_3, N_2O, HNO_3, peroxyacetyl nitrate (PAN), CH_2O, acetone, H_2O_2, CH_3OOH, HCOOH, CH_3COOH or aerosols and X is CO or CO_2) are reported as a function of plume age inferred from the progression of Δnon-methane hydrocarbons/ΔCO enhancement ratios. Emission, formation, and loss of species in plumes can be diagnosed from progression of enhancement ratios from fresh to old plumes. O_3 is produced in plumes over at least a 1 week period with mean $\Delta O_3/\Delta CO = 0.7$ in old plumes. However, enhancement ratios in plumes can be influenced by changing background mixing ratios and by photochemical loss of CO. We estimate a downward correction of ~20% in enhancement ratios in old plumes relative to ΔCO to correct for CO loss. In a case study of a large persistent biomass burning plume at 4 -km we found elevated concentrations of PAN in the fresh plume. The degradation of PAN helped maintain NO_x mixing ratios in the plume where, over the course of a week, PAN was converted to HNO_3. Ozone production in the plume was limited by the availability of NO_x, and because of the short lifetime of O_3 at 4 -km, net ozone production in the plume was negligible. Within the region, the majority of O_3 production takes place in air above median CO concentration, indicating that most O_3 production occurs in plumes. Scaling up from the mean observed $\Delta O_3/\Delta CO$ in old plumes, we estimate a minimum regional O_3 production of 17 x 10^{10}molecules O_3 $cm^{-2}s^{-1}$. This O_3 production rate is sufficient to fully explain the observed enhancement in tropospheric O_3 over the tropical South Atlantic during the dry season.

1. Introduction

Biomass burning in the tropical dry season is widespread and is thought to be increasing [*Malingreau and Tucker,* 1988; *Cahoon et al.*, 1992]. Human activities, including the burning of savannas to improve grazing, the clearing of forests and brushland for agricultural use, the use of biomass for fuel, and the burning of agricultural wastes, are the primary cause of tropical biomass burning. Emissions from biomass burning have a major influence on the photochemistry and radiation balance of the troposphere [*Crutzen et al.,* 1979; *Crutzen and Andreae,* 1990]. Emitted compounds include CO, CO_2, CH_4, nonmethane hydrocarbons (NMHCs), and nitrogen oxides ($NO_x = NO + NO_2$). The photochemical oxidation of CO and hydrocarbons in the presence of NO_x produces O_3. Tropospheric O_3 has both detrimental and advantageous effects. It is an oxidant which is damaging to vegetation and human health. In the upper troposphere it is an important greenhouse gas. However, it is also a key precursor of the hydroxyl radical (OH). OH is the primary oxidant in the troposphere and is responsible for the removal of reactive pollutants released into the atmosphere by anthropogenic and natural processes. Most oxidation of reactive long-lived gases takes place in the tropical troposphere where high insolation and humidity foster the formation of OH from the photolysis of ozone. Therefore an understanding of the influence of tropical biomass burning on tropospheric ozone production is crucial to understanding the

[1] Department of Earth and Planetary Science and the Division of Applied Science, Harvard University, Cambridge, Massachusetts.
[2] Now at National Center for Atmospheric Research, Boulder, Colorado.
[3] NASA Langley Research Center, Hampton, Virginia.
[4] Department of Chemistry, University of California at Irvine.
[5] School of Earth and Atmospheric Sciences, Georgia Institute of Technology, Atlanta.
[6] Graduate School of Oceanography, University of Rhode Island, Narragansett.
[7] NASA Ames Research Center, Moffett Field, California.
[8] Institute for the Study of Earth, Oceans and Space, University of New Hampshire, Durham.

Paper number 97JD02612.
0148-0227/98/97JD-02612$09.00

influence of tropical fires on the global oxidizing capacity of the atmosphere and on the radiative forcing of ozone in the upper troposphere.

The Transport and Atmospheric Chemistry Near the Equator-Atlantic (TRACE A) expedition was conducted during the 1992 southern tropical dry season. An overview of results from this expedition are described by *Fishman et al.* [1996] with detailed papers included in the section "Southern Tropical Atlantic Region Experiment (STARE): TRACE A and SAFARI" in *Journal of Geophysical Research, 101* (D19), 23,514-24,330, 1996. TRACE A was designed to evaluate the contribution of biomass burning to the tropospheric ozone maximum observed in satellite data off the west coast of southern Africa [*Fishman et al.*, 1990] and in seasonal enhancements of ozone concentrations measured with ozone sondes over Natal, Brazil [*Logan and Kirchhoff*, 1986]. Satellite data indicated that the magnitude of the tropospheric ozone enhancement over the South Atlantic during the burning season (August-October) is comparable to the enhancement observed in northern mid-latitudes during summer (June-August) [*Fishman et al.*, 1990]. TRACE A was coordinated with the Southern African Fire Atmospheric Research Initiative (SAFARI) which used prescribed fires and ground and low-altitude aircraft flights to characterize emissions from biomass burning fires in Africa in September-October 1992 [*Lindesay et al.*, 1996].

The TRACE A expedition made chemical and meteorological measurements during aircraft flights in the NASA DC-8 over Brazil, the South Atlantic, and southern Africa. Regions over active fires in Brazil and southern Africa, as well as continental outflow, biomass burning plumes of various ages, and clean regional background air over the south Atlantic were surveyed. Measurements in the southern hemisphere between September 22, 1992 and October 24, 1992 extended from 0°S to 38°S latitude, from 52°W to 40°E longitude, and from 0 to 12 km altitude. Flight paths are shown in Figure 1. Species measured aboard the aircraft included O_3, NO, peroxyacetyl nitrate (PAN), HNO_3, CO, CO_2, CH_4, N_2O, 35 different NMHCs, peroxides (H_2O_2 and CH_3OOH), formaldehyde (CH_2O), acetone (CH_3COCH_3), formic and acetic acids (HCOOH, CH_3COOH), aerosol density and size distribution, and several chlorinated compounds of exclusively industrial origin including C_2Cl_4, CH_3CCl_3, CFC-11, CFC-12, and CFC-113. Meteorological parameters, UV radiation, temperature and dew point were also measured.

Extensive research has been conducted in the field and laboratory to characterize emissions from biomass burning in both temperate [*Cofer et al.*, 1989, 1990; *Hegg et al.*, 1990; *Laursen et al.*, 1992; *Lobert et al.*, 1991; *Yokelson et al.*, 1996] and tropical regions [*Greenberg et al.*, 1984; *Hurst et al*, 1994a, 1994b; *Bonsang et al.*, 1991, 1995; *Lacaux et al.*, 1995; *Helas et al.*, 1995; *Rudolph et al.*, 1995; *Cofer et al.*, 1996; *Hao et al.*, 1996]. Efforts to determine enhancement ratios of tracers of biomass combustion have also been made from measurements collected during other large integrated aircraft expeditions such as Amazon Boundary Layer Experiment (ABLE) 2A in the dry season over the Brazilian rainforest [*Andreae et al.*, 1988], Arctic Boundary Layer Expedition (ABLE) 3A over the Alaskan arctic in summer [*Wofsy et al.*, 1992, 1994], Arctic Boundary Layer Expedition (ABLE) 3B over eastern Canada in summer [*Blake et al.*, 1994; *Wofsy et al.*, 1994; *Mauzerall et al.*, 1996], Chemical Instrumentation Test and Evaluation (CITE) 3 during the dry season over the equatorial and tropical south Atlantic [*Andreae et al.*, 1994], Dynamique et Chimie Atmospherique en Foret Equatoriale (DECAFE) over the Ivory Coast in the dry season [*Bonsang et al.*, 1995; *Delmas et al.*, 1995; *Helas et al.*, 1995; *Rudolph et al.*, 1995], SAFARI over southern African savannas [*Ward et al.*, 1996; *Hao et al.*, 1996; *Lacaux et al.*, 1996; *Cofer et al.*, 1996; *Andreae et al.*, 1996] and TRACE A [*Blake et al.*,

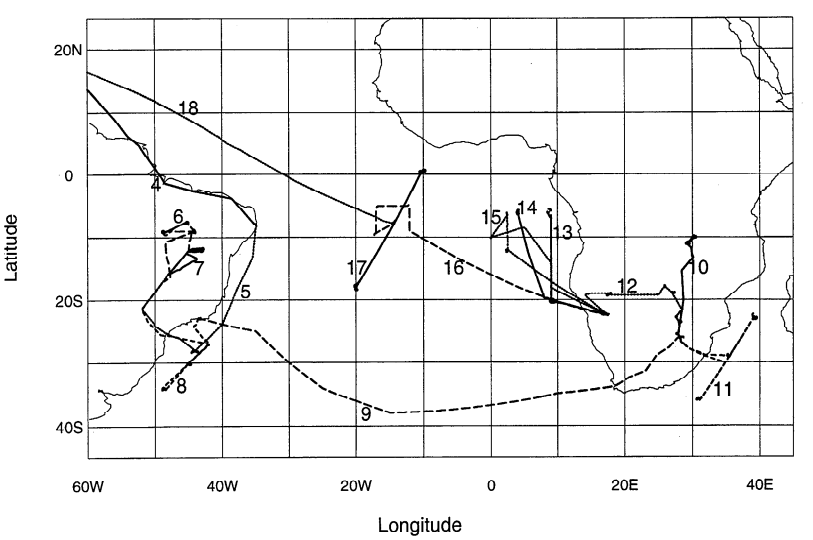

Figure 1. Transport and Atmospheric Chemistry near the Equator-Atlantic (TRACE A) flight paths used in analysis (September 22, 1992 - October 24, 1992). Numbers on the map indicate individual flights.

1996; *Pickering et al.*, 1996, *Lee et al.*, 1997]. *Chatfield et al.* [1996] have examined the evolution of an idealized African biomass burning plume using a two-dimensional (2-D) model. Although other work has examined aged biomass burning emissions and their impact on the TRACE A region [*Browell et al.*, 1996; *Gregory et al.*, 1996; *Singh et al.*, 1996; *Smyth et al*, 1996; *Talbot et al*, 1996; *Thompson et al.*, 1996] less work has focussed on how biomass burning emissions evolve in plumes as they photochemically age, or on the contribution of O_3 production in plumes to the regional O_3 enhancement. In this paper we address these issues.

This paper is organized into five sections. In section 2 we describe a method of classifying plumes by photochemical age and we examine the temporal evolution of enhancement ratios ($\Delta Y/\Delta X$) of photochemical tracers in the TRACE A plumes. We also discuss the influence of changing background concentrations and photochemical loss of CO on enhancement ratios. Section 3 is a case study of a large biomass burning plume sampled off the west coast of Africa. In section 4 we examine the influence that the dispersal of biomass burning plumes has on regional ozone production. Results of our analysis are summarized in section 5.

2. Data Analysis

2.1. Identification of Plumes and Determination of Enhancement Ratios

We identified biomass burning plumes sampled during the TRACE A expedition in time series plots of CO mixing ratio using the criteria that a plume exhibit an enhancement of at least 20 ppbv CO relative to local background. Concurrent enhancements in other emitted species including CO_2 and C_2H_2 were used for confirmation. Enhancements in halocarbon concentrations (e.g. C_2Cl_4 and CH_3CCl_3) identified urban pollution plumes (flight 5 along the east coast of Brazil and flight 8 returning to Rio de Janeiro), and these plumes were discarded. For each plume, least square regressions of every species were calculated relative to CO and CO_2, and the slope of each regression was obtained using the reduced-major-axis method [*Hirsch and Gilroy*, 1984]. The slope provides the enhancement ratio in the plume relative to the local background ($\Delta Y/\Delta X$). Statistically significant regressions were diagnosed using a t -test with 95% confidence limits. In order to exclude regressions which appeared statistically significant due to a large number of observations but which actually included two separate populations of points $r^2 > 0.3$ was also required.

We based our analyses on merged time series of aircraft measurements where all the data were averaged over a common time interval. In TRACE A the frequency and time resolution of measurements varied considerably. Measurements for some species were reported with 5 -second resolution (CO, CO_2, CH_4, and N_2O), while averaging times were longer for other species (10 seconds for O_3, 60 seconds for CH_2O, 90 seconds for NO, 130 seconds for acetone, and 150 seconds for PAN). For still other species the frequency of measurements and the sampling interval were variable (NMHCs and halocarbons, H_2O_2, and HNO_3). We chose to average the data over the measurement time interval of the critical species with coarsest time resolution. Depending on the question we are addressing, the critical species changes. We therefore use eight different merges matching the sampling time interval of particular species: 10- second merge (CO, CO_2, CH_4, N_2O, and O_3), 60- second merge (CH_2O), 90- or 180- second merge (NO), 130- second merge (acetone), 150- second merge (PAN), and three variable-time merges (NMHCs, HNO_3, H_2O_2).

2.2. Plume Classification and Locations

The temporal evolution of enhancement ratios is a function of both photochemistry and plume dilution [*McKeen and Liu*, 1993]. NMHCs provide a diagnostic of the relative age of plumes, with significant correlations between short-lived NMHCs and CO present only in relatively fresh plumes and correlations between longer-lived NMHCs and CO being maintained in older plumes. We classified biomass burning plumes into four age categories using the presence or absence of enhancement ratios for 10 NMHCs with a range of lifetimes (as shown in Table 1) to CO. Table 2 gives mean enhancement ratios relative to CO (ΔNMHC/ΔCO) for hydrocarbons used to assign relative plume ages

Table 1. Typical Lifetimes of O_3 and Nonmethane Hydrocarbons (NMHCs) in Transport and Atmospheric Chemistry Near the Equator-Atlantic (TRACE A)

	0-4 km	4-8 km	8-12 km
Temperature, K	284	258	230
OH,[a] molecules cm^{-3}	2.7×10^6	1.6×10^6	1.2×10^6
Species	*Lifetime,[b] days*		
O_3	6	25	105
Isoprene	0.04	0.05	0.06
1-Butene	0.09	0.13	0.14
Propene	0.15	0.25	0.33‘
Ethene	0.5	0.9	1.2
Toluene	0.7	1.0	1.1
n-Butane	1.8	3.4	5.3
Benzene	3.5	6.3	9.2
Propane	4.3	8.9	16
Acetylene	6.5	13	23
Ethane	20	48	100

[a] Mean values calculated for TRACE A conditions as determined by Jacob et al. [1996].

[b] Lifetimes were calculated on the basis of oxidation by OH only.

Table 2. Mean Hydrocarbon Enhancement Ratios in Plumes (pptv/ppbv)

	Fresh Plumes (11)			Recent Plumes (10)			Aged Plumes (16)			Old Plumes (14)		
	Mean	Standard Error	Significant Plumes[a]	Mean	Standard Error	Significant Plumes[a]	Mean	Standard Error	Significant Plumes[a]	Mean	Standard Error	Significant Plumes[a]
ΔIsoprene / ΔCO	0.29	± 0.031	3	NA		0	NA		0	NA		0
Δ1-Butene / ΔCO	0.24	± 0.12	5	NA		0	NA		0	NA		0
ΔPropene / ΔCO	1.18	± 0.47	8	NA		0	NA		0	NA		0
ΔEthene / ΔCO	6.88	± 1.34	8	1.32	± 0.27	7	NA		0	NA		0
ΔToluene / ΔCO	0.67	± 0.10	8	0.24		1	NA		0	NA		0
Δn-Butane / ΔCO	0.33	± 0.11	5	0.20	± 0.09	3	0.23	± 0.10	5	NA		0
ΔBenzene / ΔCO	1.30	± 0.06	8	0.81	± 0.054	8	0.48	± 0.048	13	NA		0
ΔPropane / ΔCO	2.35	± 0.82	8	0.97	± 0.15	4	1.22	± 0.43	10	NA		0
ΔC_2H_2 / ΔCO	4.22	± 0.37	8	3.40	± 0.47	8	2.62	± 0.15	15	2.82	± 0.18	14
ΔC_2H_6 / ΔCO	7.53	± 0.63	8	5.87	± 0.69	5	7.07	± 1.07	14	8.02	± 0.71	8

The total number of plumes in a given age category is in parentheses. Enhancement ratios in each plume category include the mean and the standard error ($\sigma/\sqrt{n}$).

[a] The number of plumes with statistically significant correlations. When that number is zero, NA is entered for the mean and standard error.

for each of the four age categories. For a particular ΔNMHC/ΔCO a systematic decrease in slope from one age category to the next is usually observed because of the more rapid disappearance of the NMHC than of the CO. As plumes age, enhancements of short-lived hydrocarbons progressively disappear. Significant enhancements of at least one NMHC with a lifetime at low altitudes of < 0.2 days (isoprene, 1-butene, or propene) was required to categorize a plume as fresh; between 0.5 and 1-day (ethene or toluene) was required to categorize a plume as recent; between 2 and 5 days (*n*-butane, benzene, or propane) was required to categorize a plume as aged; and > six days (acetylene or ethane) was required to categorize a plume as old. The ages of individual plumes were also estimated independently from advanced very high resolution radiometer (AVHRR) satellite imagery of fire locations in combination with meteorological back trajectories. Fresh plumes were typically less than half a day old, recent plumes were < 1 day old; aged plumes were < five days old; and old plumes were < 1 week old.

Figure 2 presents examples of a plume in each age category ((a) fresh, (b) recent, (c) aged, and (d) old). For each age category a time series of selected data from a flight segment is shown. Vertical lines on the time series indicate the interval identified as containing a plume. Scatter plots of the data within the time interval of the plume are shown with superimposed lines indicating a significant correlation between the plotted species. Slopes of these lines provide enhancement ratios.

The locations of individual plumes are shown on the regional map in Figure 3a, while the altitude of the CO maximum of individual plumes is shown versus longitude in Figure 3b. Fresh plumes are directly over source regions and are typically within the boundary layer. Recent plumes are also usually directly over the source regions but are generally within the free troposphere. Aged plumes can be found over both the continents and the Atlantic at any altitude but are usually in the free troposphere. Old plumes are found remote from continental source regions in the free troposphere.

2.3. Analysis of Enhancement Ratios

Previous analyses of biomass burning have characterized biomass burning emissions by determining the ratio of $\Delta Y/\Delta X$ (where Y is a compound either emitted by the fire or produced in the fire plume, X is a reference tracer assumed to be conserved in the plume (usually CO or CO_2), and Δ indicates the mixing ratio of a compound in the plume minus the mixing ratio in local background air). The chemical composition of the plume is characterized by the regression slope of Y versus X. Emission ratios of this type have been used in combination with estimates of the amount of biomass burned to quantify the contribution of biomass burning to trace gas budgets for CO, CH_4, NO_x, and other gases [*Crutzen et al.*, 1979; *Crutzen and Andreae*, 1990; *Laursen et al.*, 1992]. A similar approach has also been employed to estimate photochemical production of ozone by assuming that $\Delta O_3/\Delta CO$ indicates the number of ozone molecules produced per CO molecule emitted during combustion [*Parrish et al.*, 1993, *Andreae et al.*, 1994]. In this study we examine the validity of this approach.

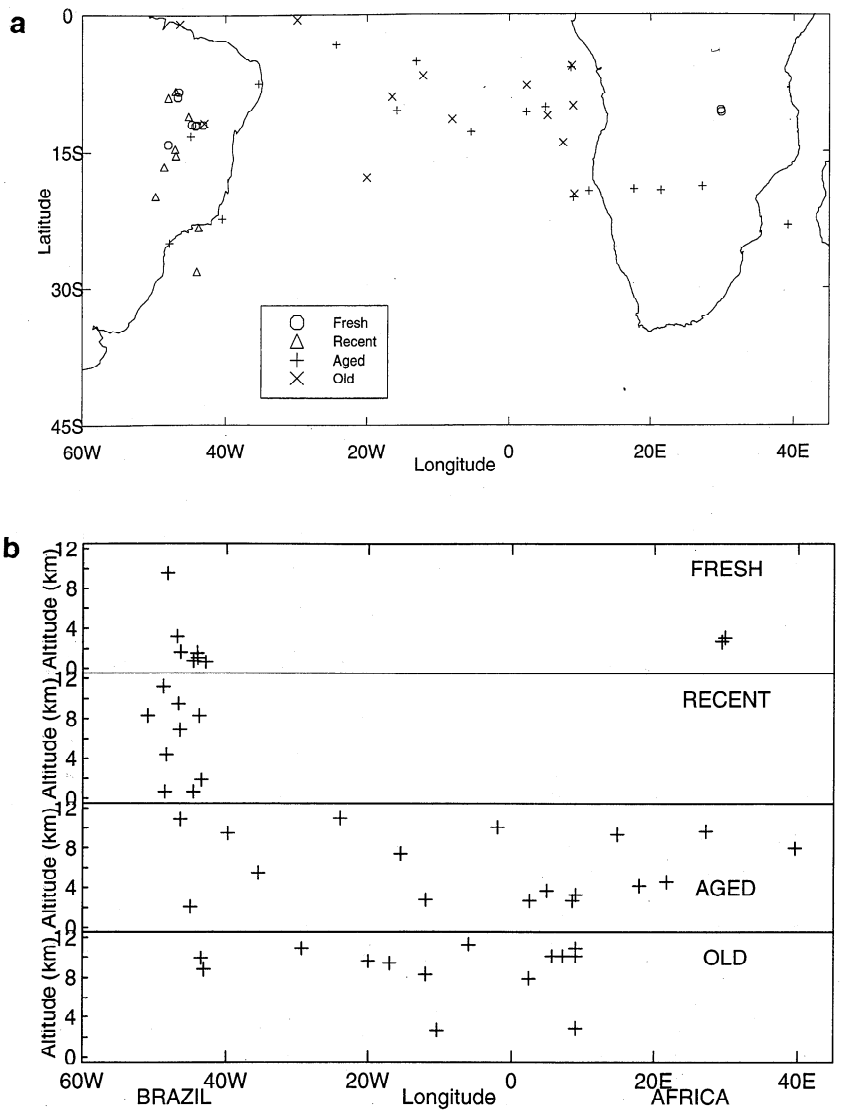

Figure 2. (a) Map of fresh, recent, aged and old plume locations. (b) Vertical locations of fresh, recent, aged and old plumes. Plus marks indicate maximum CO mixing ratio for a given plume.

Tables 3a and 3b present enhancement ratios relative to CO and CO_2 for a number of species: O_3, CH_4, N_2O, CH_3Cl, HNO_3, PAN, CH_2O, $(CH_3)_2CO$, H_2O_2, CH_3OOH, HCOOH, CH_3COOH, and aerosols. We examine enhancement ratios versus both CO and CO_2 because each compound has particular advantages and disadvantages. CO_2 is chemically inert in the atmosphere but exchanges with the biosphere; it also has a large background concentration which can make small enhancements difficult to detect above natural variability. CO, emitted primarily during smoldering combustion, is an attractive reference because it correlates well with other partially oxidized and reduced compounds emitted during similar combustion regimes. It is not taken up by vegetation, and its background mixing ratio is 3 orders of magnitude lower than CO_2, making detection of combustion plumes easier. However, CO is not chemically inert.

We observe that as plumes age $\Delta CO/\Delta CO_2$ decreases, with the most appreciable decrease between fresh and recent aged plumes (see Table 3b). There are two possible explanations for this decrease. First, background mixing ratios are not the same in all plume age categories (see Table 4). Second, there is photochemical loss of CO over the lifetime of the plume. These two factors have implications for all enhancement ratios and will be discussed, in turn, below.

2.3.1. Implications of changing background mixing ratios. A limitation on the use of enhancement ratios is imposed by variable background mixing ratios. In environments where background mixing ratios vary from one location to another, enhancement ratios of a particular pair of species relative to their local background mixing ratios vary as a plume dilutes [*McKeen and Liu,* 1993]. To illustrate this point, we show in Figure 4a the schematic of a fire plume containing two inert species with concentrations (x_p', y_p') and diluting with background air of composition (x_b', y_b') that is different from the background air at the point of emission (x_b, y_b) in which the fresh plume (x_p, y_p) formed. Let R be the emission ratio of y to x in the fire. Linear regression of concentration measurements within the fresh plume

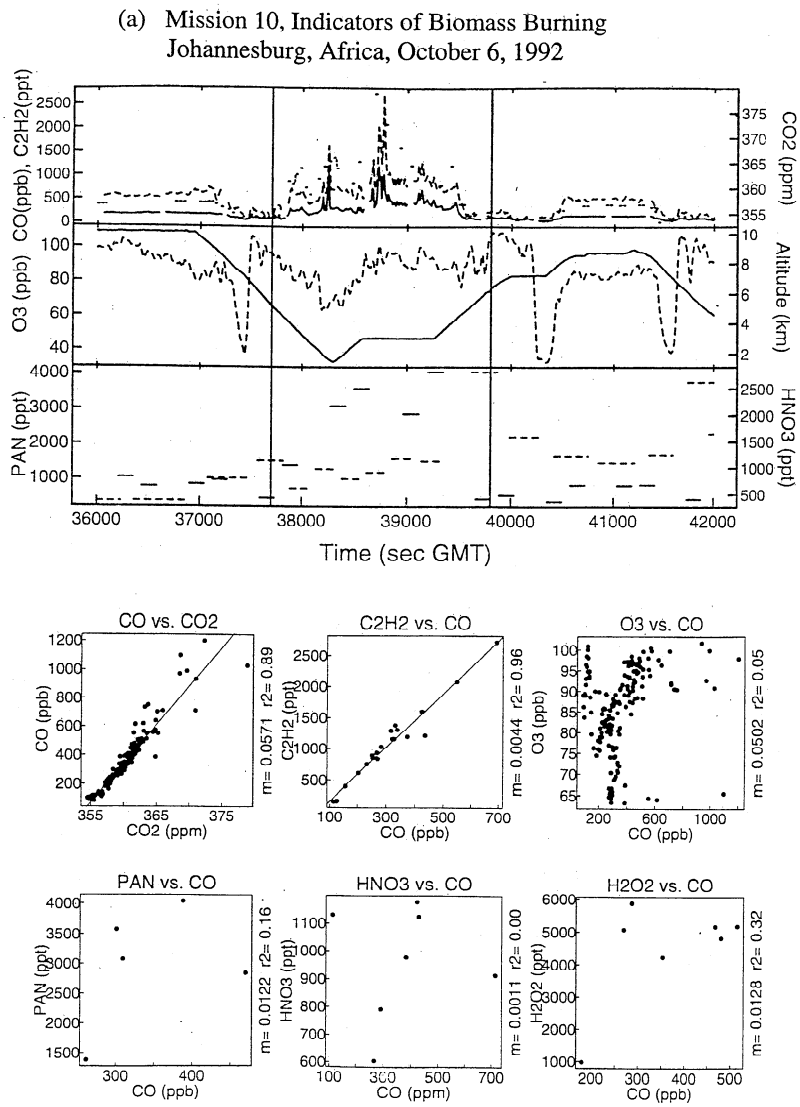

Figure 3. Examples of plume identification and determination of enhancement ratios. Time series and selected correlations are shown for examples of (a) fresh, (b) recent, (c) aged, and (d) old plumes. In Figures 3a-3d, a set of time series is plotted on the top half of the page. CO, altitude and peroxyacetyl nitrate (PAN) are plotted with solid lines; CO_2, O_3 and HNO_3 are plotted with dashed lines; and C_2H_2 is plotted with a dotted line. The minimum criteria used to define a plume was an enhancement of at least 20 ppbv CO above local background concentrations. A plume includes all data from this local minimum to the locally observed maximum. Plumes are shown as the data between the vertical lines on the time series. Over the time interval of a plume, measurements of all species were extracted and regressions of every species versus CO and CO_2 were calculated. Here, correlations for CO versus CO_2, and for C_2H_2, O_3, PAN, HNO_3, and H_2O_2 versus CO are shown. Lines representing the reduced-major-axis regression are drawn on each plot if a t test indicates 95% confidence and $r^2 > 0.3$. The slopes, m, of statistically significant regressions are the enhancement ratios.

yields a slope of $R = \Delta y/\Delta x$ representing the emission ratio from the fire. However, as the plume dilutes with background air of changing composition, the slope will change (Figure 4b), biasing the interpretation of enhancement ratios in the plume relative to the emission ratio. For all cases of interest here, with $x_b - x_b' > 0$ and $y_b - y_b' > 0$, the bias is negative (i.e., $(y_b - y_b') / (x_b - x_b') < R$). This largely explains the dramatic decrease in $\Delta CO/\Delta CO_2$ from the fresh to the recent plume age categories.

2.3.2. Chemical loss of CO. Photochemical loss of CO is also responsible, in part, for the decrease in $\Delta CO/\Delta CO_2$ as plumes age. We calculated CO lifetimes (Figure 5) using mean model OH values reported for the TRACE A conditions at different altitudes by *Jacob et al.* [1996]. Results indicate a CO lifetime of about 20 days below 6 -km altitude, rising to 60 days at 12 km. Below 6 -km the lifetime of CO is short enough that over a 1 week transit time, one -third of the CO in a plume may be lost. Thus photochemical loss of

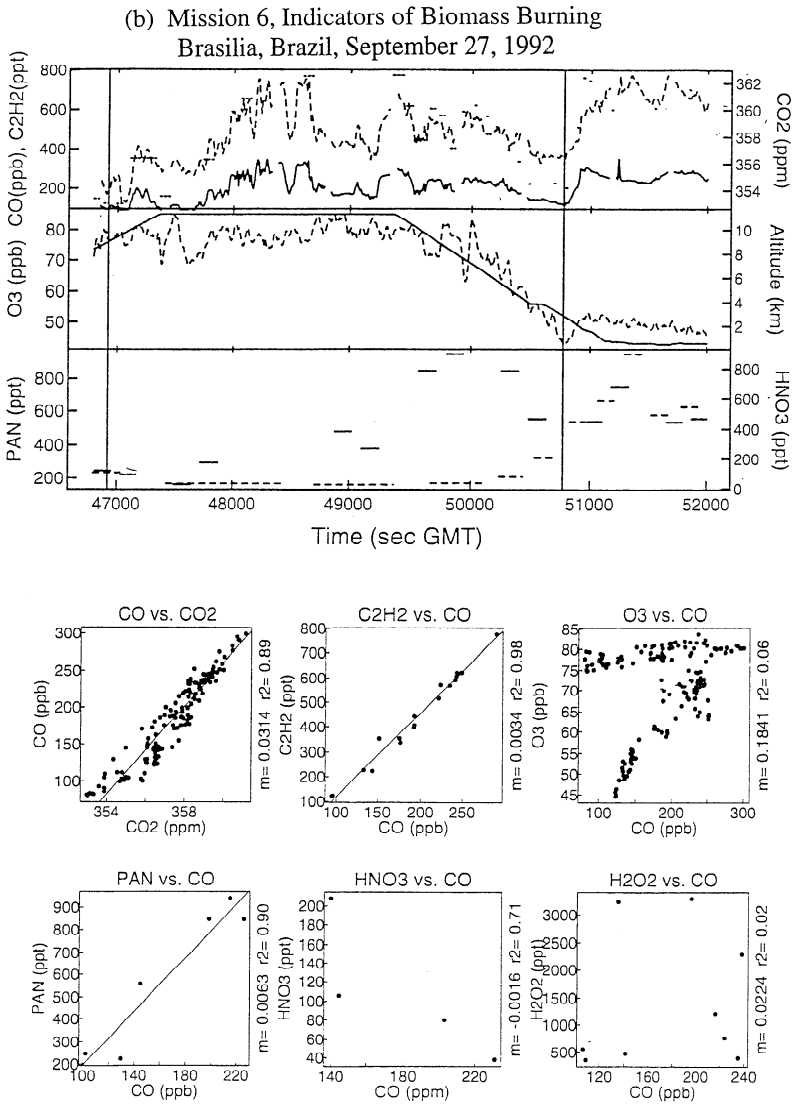

Figure 3. (continued)

CO contributes to a decrease in $\Delta CO/\Delta CO_2$ as well as to an upward bias on enhancement ratios of $\Delta X/\Delta CO$ (where X is any chemical species).

2.4. Photochemical Evolution of Plumes Determined From Enhancement Ratios

Through an examination of the mean enhancement ratios relative to CO and CO_2 shown in Table 3 we can gain insight into which species are emitted from the fire and which are produced through oxidation processes in the plume. Species which exhibit strong correlations with CO in fresh plumes and weaker correlations as plumes age and which have enhancement ratios which decrease as plumes age are presumably emitted from the fire or formed in the fresh plume. Species which show increasing correlation with CO and enhancement ratios which increase more rapidly than can be explained by the loss of CO as plumes age are presumably produced gradually in the plumes.

2.4.1. Ozone. For the TRACE A region, as shown in Table 3, $\Delta O_3/\Delta CO$ increases from 0.15 to 0.32 to 0.71 to 0.74 ppbv/ppbv in fresh, recent, aged, and old plumes, respectively. These values can be compared to previously reported biomass burning $\Delta O_3/\Delta CO$ values of 0.056 ppbv/ppbv in the Amazon basin, of 0.06 ppbv/ppbv in North America and of 0.46 ppbv/ppbv over the South Atlantic [*Andreae et al.*, 1994]. However, this study is the first time that plumes have been segregated on the basis of age. The range observed here is similar to that reported by *Andreae et al.* [1994]. Photochemical loss of CO in the plumes causes ΔCO to be smaller and $\Delta O_3/\Delta CO$ to be larger than they would be if CO were an inert tracer. Aged plumes at lower altitudes may exhibit a $\Delta O_3/\Delta CO$ as much as 30% higher than would have been observed were CO inert. At higher altitudes, because of lower OH concentrations, CO loss is not as rapid, and the correction is less. Changes in the background O_3 and CO mixing ratios conversely cause a downward bias on $\Delta O_3/\Delta CO$ as plumes age from fresh to recent categories, but because CO enhancements in fresh plumes are so large relative to the change in the background, the downward bias will be small, and the influence of changes in the background become neg-

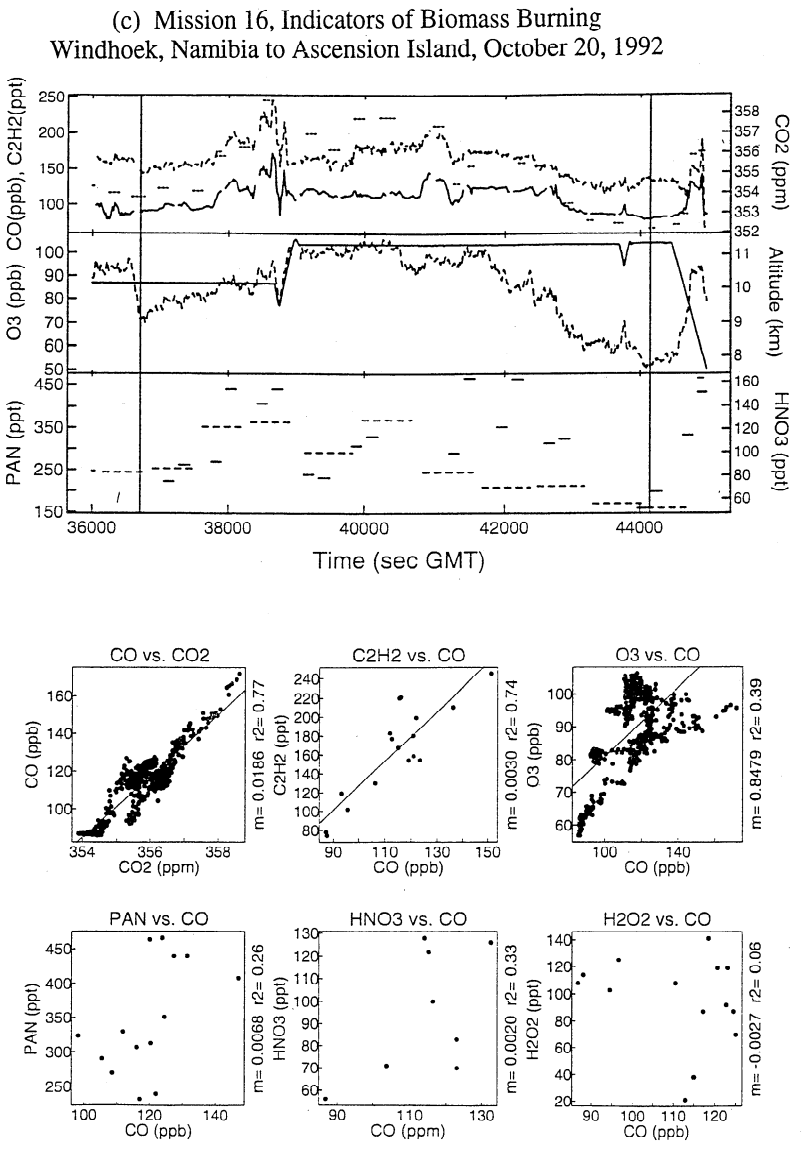

Figure 3. (continued)

ligible when considering further aging (see Table 4). We therefore estimate a downward correction of 20% in $\Delta O_3/\Delta CO$ in old plumes because of the photochemical loss of CO.

2.4.2. NO_x. We calculate ΔNO_x in the plumes by combining measurements of NO with NO_2 values calculated using a point model (see *Jacob et al.*, [1996] for a description of the model). The $\Delta NO_x/\Delta CO$ ratio in fresh plumes of 5.2 pptv/ppbv is similar to the 3.4 pptv/ppbv ratio observed previously in boreal biomass fires over Alaska [*Wofsy et al.*, 1992] but is low relative to the range 2 - 50 pptv/ppbv reported in the review by *Crutzen and Andreae* [1990]. The $\Delta NO_x/\Delta CO$ ratio in recent, aged, and old plumes remains relatively constant near 3 pptv/ppbv, possibly sustained by decomposition of PAN to NO_x and subsequent conversion of NO_x to HNO_3. Because of relatively sparse measurements and the aggregation of plumes which have travelled at a variety of altitudes, the progression of $\Delta PAN/\Delta CO$ and $\Delta HNO_3/\Delta CO$ do not reflect the conversion of PAN to HNO_3. However, the case study we discuss in section 3 exemplifies this conversion.

2.4.3. Methane. CH_4 is emitted from fires and because of its long atmospheric lifetime is conserved over the lifetime of the plumes. Values of $\Delta CH_4/\Delta CO$ slowly increase as the plumes age because of loss of CO, while $\Delta CH_4/\Delta CO_2$ remains effectively constant over the lifetime of the plumes. However, as shown in Figure 6a, median mixing ratios of CH_4 increase with altitude in the TRACE A region at a rate of 2.3 ppbv/km [*Bartlett et al.*, 1996]. *Krishnamurti et al.* [1993] estimate a regional descent rate of upper tropospheric air to 900 mb of about 5 days. Thus northern hemisphere air carried to the upper troposphere in the Hadley cell circulation and subsiding in the southern hemisphere tropics likely contributes to the upper tropospheric enhancement in CH_4. In addition, we calculate a median photochemical lifetime for CH_4 which increases with altitude (Figure 6b). Despite

(d) Mission 17, Indicators of Biomass Burning
Local Flight, Ascension Island, October 22, 1992

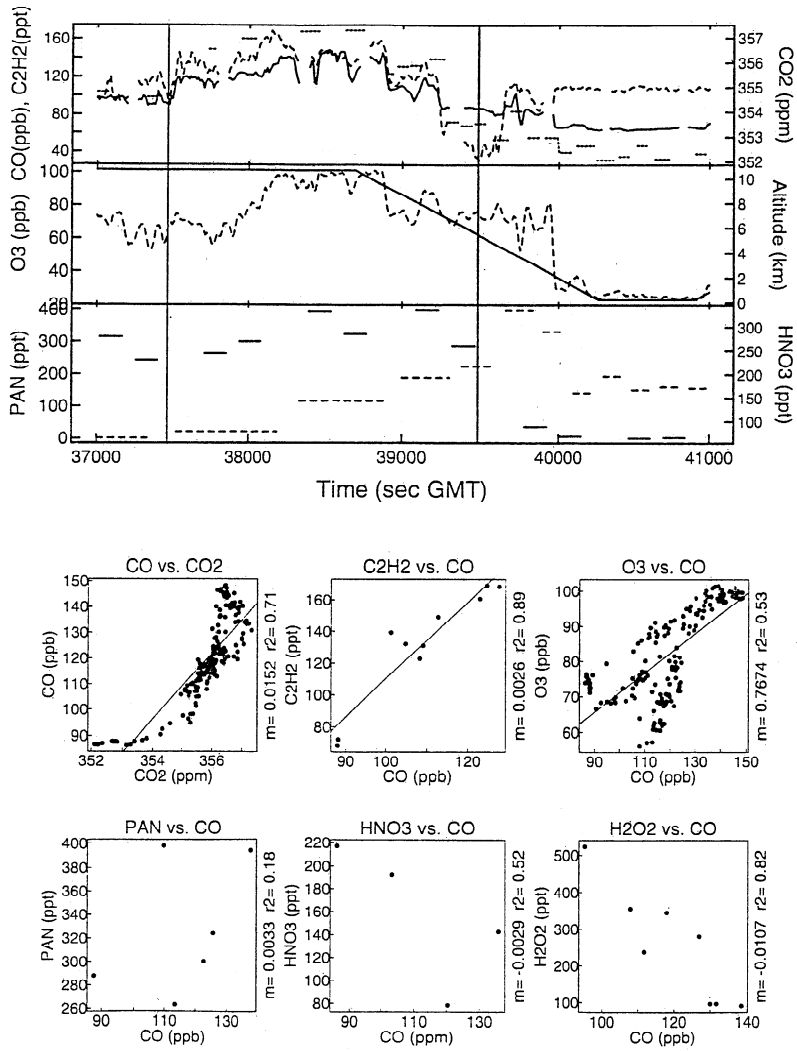

Figure 3. (continued)

rapid downward mixing of upper tropospheric air in this region, loss rates of 2 ppbv/day in the lower troposphere likely also contribute to the observed vertical gradient of CH_4 mixing ratio by providing a larger sink at lower altitudes.

2.4.4. Formaldehyde. Examining enhancement ratios for the four plume age categories, we find the largest fraction of significant correlations (55% of plumes) of $\Delta CH_2O/\Delta CO$ in fresh plumes and the smallest fraction (7%) in old plumes. In addition, there is a progressive decrease in the slope of the mean enhancement ratios as the plumes age from 0.0095 in fresh plumes to 0.0009 in old plumes This indicates that CH_2O is emitted from the fire or formed shortly thereafter from the oxidation of short-lived hydrocarbons and then progressively lost as the plumes age. Direct emission of CH_2O in biomass burning is confirmed by *Lee et al.* [1997].

2.4.5. Peroxides. Examining enhancement ratios (Table 3) for the four plume age categories, we do not find as clear a signature for initial production of peroxides within the fire as we did for CH_2O. Only 33% of the correlations in fresh plumes were significant for H_2O_2, and none were significant for CH_3OOH. The fraction of plumes in the recent and aged categories which exhibited significant correlations for $\Delta H_2O_2/\Delta CO$ and $\Delta CH_3OOH/\Delta CO$ never exceeded 30% and were < 10% in old plumes. The lifetimes of the peroxides against photolysis and reaction with OH are typically < 1 day (see section 3). The fact that significant correlations did not entirely disappear indicates that the net photochemical production of peroxides in the plumes was sufficient to maintain H_2O_2 mixing ratios enhanced over the background and to produce CH_3OOH.

2.4.6. Acetone. A biomass burning source of acetone was identified in boreal biomass fires by *Singh et al.* [1994], and when all TRACE A acetone measurements are plotted versus CO, a strong positive correlation results, indicating a regional biomass burning source of acetone (see Figure 7). However, examining enhancement ratios (Table 3) for the four plume age categories, we find no significant enhancements in fresh plumes and significant enhancement ratios in

Table 3a. Mean Photochemical Enhancement Ratios Relative to CO in Plumes

	Fresh Plumes (11)			Recent Plumes (10)			Aged Plumes (16)			Old Plumes (14)		
	Mean	Standard Error	Significant Plumes[a]	Mean	Standard Error	Significant Plumes[a]	Mean	Standard Error	Significant Plumes[a]	Mean	Standard Error	Significant Plumes[a]
ΔO_3 / ΔCO	0.15	± 0.37	4	0.32	± 0.76	4	0.71	± 0.12	10	0.74	± 0.9	8
ΔCH_4 / ΔCO	0.16	± 0.05	10	0.37	± 0.003	2	0.6	± 0.076	7	0.44	± 0.12	5
ΔN_2O / ΔCO	0.002		1	0.022		1	0.028		1	0.012		1
ΔCH_3Cl / ΔCO	0.77	± 0.08	8	0.85	± 0.04	8	1.21	± 0.12	14	1.43	± 0.13	8
ΔNO_x[b] / ΔCO	5.2	± 0.64	4	3.8	± 2.8	2	2.7	± 1.5	7	3.3	± 1.4	3
ΔHNO_3 / ΔCO	2.2	± 0.49	2	5.8		1	5.1	± 0.3	2	NA		0
ΔPAN / ΔCO	6.0	± 1.7	3	7.5	± 1.6	4	5.3	± 0.45	5	6.0	± 0.3	2
ΔCH_2O / ΔCO	9.5	± 0.65	6	1.8	± 0.81	3	2.3	± 0.7	3	NA		0
ΔAcetone / ΔCO	NA		0	10.3	± 1.9	3	7.7	± 1.2	5	7.2	± 1.7	3
ΔH_2O_2 / ΔCO	11.8	± 0.6	2	68.0	± 44.9	2	39.1	± 11.3	4	20.8	± 17.8	3
ΔCH_3OOH / ΔCO	2.5		1	15.5	± 6.8	3	16.3	± 2.8	4	10.6	± 7.1	2
ΔHCOOH / ΔCO	14.7	± 4.6	3	43.1	± 3.6	2	28.4	± 8.9	3	NA		0
ΔCH_3COOH / ΔCO	16.5	± 1.6	4	106.5		1	18.2	± 9.2	2	NA		0
Δ (0.12- 3.12um Aerosols) / ΔCO	18.2	± 1.85	10	14.8	± 3.25	5	7.59	± 2.1	7	4.6	± 2.4	7

Units are ppbv/ppbv for $\Delta O_3/\Delta$CO, $\Delta CH_4/\Delta$CO and $\Delta N_2O/\Delta$CO and are pptv/ppbv for all other ratios. The total number of plumes in a given age category is in parentheses in the top row. Enhancement ratios in each plume category include the mean and the standard error ($\sigma/\sqrt{n}$).

[a] The number in parentheses gives the total number of plumes with statistically significant correlations; when that number is zero, NA is entered for the mean and standard error.

[b] $NO_x = (NO)_{measured} + (NO_2)_{calculated}$. NO_2 is calculated for every point in the plume using a point model and assuming diurnal steady state [*Jacob et al.*, 1996].

Table 3b. Mean Photochemical Enhancement Ratios Relative to CO_2 in Plumes

	Fresh Plumes (11)			Recent Plumes (10)			Aged Plumes (16)			Old Plumes (14)		
	Mean	Standard Error	Significant Plumes[a]	Mean	Standard Error	Significant Plumes[a]	Mean	Standard Error	Significant Plumes[a]	Mean	Standard Error	Significant Plumes[a]
$\Delta CO / \Delta CO_2$	47.4	± 6.4	10	23.2	± 2.0	10	21.3	± 1.2	13	16.1	± 1.9	13
$\Delta CH_4 / \Delta CO_2$	4.6	± 1.2	8	9.		1	9		1	5.2	± 0.5	5
$\Delta O_3 / \Delta CO_2$	5.1	± 2.	4	8.6	± 1.1	3	12.4	± 1.7	6	12.5	± 2.6	5
$\Delta N2O / \Delta CO_2$	0.14		1	0.56		1	0.24		1	NA		0
$\Delta NO_x / \Delta CO_2$	0.16	± 0.063	4	0.014		1	0.07	± 0.04	7	0.05	± 0.01	5
$\Delta HNO_3 / \Delta CO_2$	0.1		1	0.17		1	0.07	± 0.02	5	NA		0
$\Delta PAN / \Delta CO_2$	0.25	± 0.14	3	0.18	± 0.014	3	0.14	± 0.03	4	0.09	± 0.026	3
$\Delta CH_2O / \Delta CO_2$	0.57	± 0.056	4	0.044	± 0.02	3	0.05	± 0.01	3	NA		0
ΔAcetone / ΔCO_2	NA		0	0.18		1	0.13		1	0.11	± 0.002	2
$\Delta H_2O_2 / \Delta CO_2$	0.55	± 0.13	2	1.91	± 1.14	2	1.78	± 0.62	5	1.22		1
$\Delta CH_3OOH / \Delta CO_2$	0.42	± 0.29	3	0.40	± 0.21	3	0.42	± 0.056	5	0.38		1
$\Delta HCOOH / \Delta CO_2$	0.64	± 0.21	4	0.99	± 0.37	2	0.55	± 0.20	3	0.23		1
$\Delta CH_3COOH / \Delta CO_2$	0.79	± 0.23	4	NA		0	0.71		1	NA		0
Δ(0.12- 3.12um Aerosols) / ΔCO_2	0.86	± 0.15	6	0.3	± 0.11	4	0.15	± 0.05	6	0.063	± 0.035	9

[a] Units are ppbv/ppmv for $\Delta CO/\Delta CO_2$, $\Delta CH_4/\Delta CO_2$ and $\Delta N_2O/\Delta CO_2$ and are pptv/ppmv for all other ratios. See Table 3a for further explanations.

Table 4. Mean Background Mixing Ratios

	Fresh Plumes (11)	Recent Plumes (10)	Aged Plumes (16)	Old Plumes (14)
CO, ppbv	139 ± 11	87 ± 10	79 ± 3.5	83 ± 2.9
CO_2, ppmv	356 ± 0.4	354 ± 0.4	354 ± 0.3	352.8 ± 0.2
O_3, ppbv	49 ± 3.5	44 ± 4	41 ± 4.5	49 ± 4

The total number of plumes in a given age category is in parentheses. Mean background mixing ratios and the standard error ($\sigma/\sqrt{n}$) are shown for every age category for each compound. Background mixing ratios were obtained by averaging the local minimum concentrations observed on either side of the plumes within each age category.

only about 25% of the older age categories, reflecting, we believe, the relatively sparse acetone measurements. The data suggest that acetone is formed as a secondary product in the plume, possibly from the oxidation of propane (see section 3).

3. African Plume Case Study

On October 14-18 the TRACE A aircraft sampled a large biomass burning plume transported from the west coast of Africa to the Atlantic Ocean. The plume extended from the top of the marine boundary layer (1.5 km altitude) to ~5.5 km. Flights 13 and 14 were designed to sample this plume 1 day downwind of each other. Flight 15 sampled the same plume again 3 days after flight 14. AVHRR data for October 12, 1992 (Plate 1) and 5 day back trajectories for flights 13 (Figure 8a), 14 (Figure 8b) and 15 (Figure 8c) indicate that air parcels for these flights last passed over burning areas on October 12, 1992, 2, 3, and 5 days before they were intercepted by the aircraft. Although the origin of the emissions sampled in mission 10 (used to initialize the calculation) was east of the origin of the emissions sampled in missions 13, 14, and 15, the African ecosystem at this latitude is primarily grassy and woody savanna [*Lavenu*, 1987], and drought conditions prevailed in both areas. We therefore assume that the time since emission is the most critical factor determining plume composition.

3.1. Evolution of NO_y Partitioning

In Plate 2 we show vertical profiles of CO, HNO_3, PAN, and NO_x mixing ratios in the plume sampled during mis-

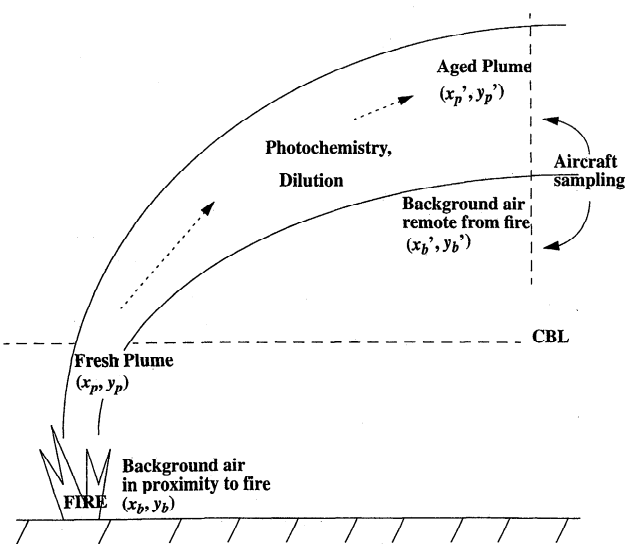

Figure 4a. Schematic of plume formation and transport. The (x_p, y_p) and (x_b, y_b) indicate mixing ratios within the fresh plume at the time of sampling and in background air in proximity to the fire, respectively. The (x_p', y_p'), and (x_b', y_b') indicate mixing ratios within the plume sampled by the aircraft and in background air in the vicinity of the sampled plume, respectively.

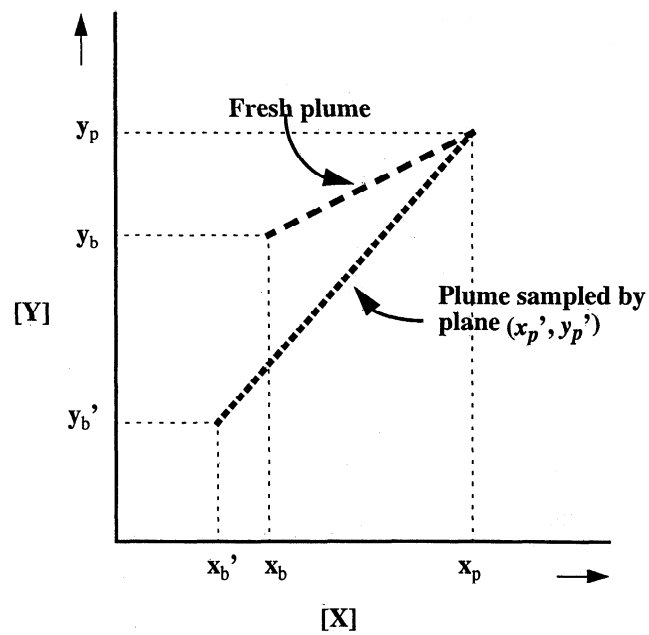

Figure 4b. Schematic of plume sampling. Long-dashed line indicates a fresh plume with enhancements (x_p-x_b, y_p-y_b) relative to background mixing ratios near the fire (x_b,y_b). Dotted line indicates a plume remote from the fire which the aircraft measures relative to local background mixing ratios (x_b', y_b'). Enhancement ratios are obtained from the slopes of these lines.

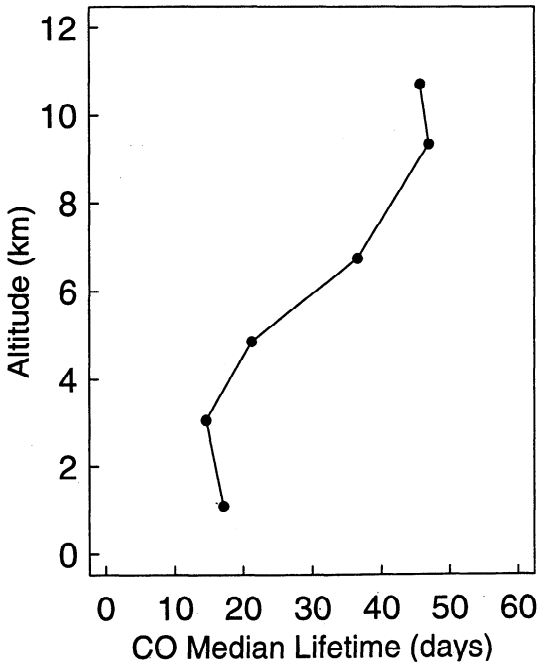

Figure 5. Median CO lifetime versus altitude.

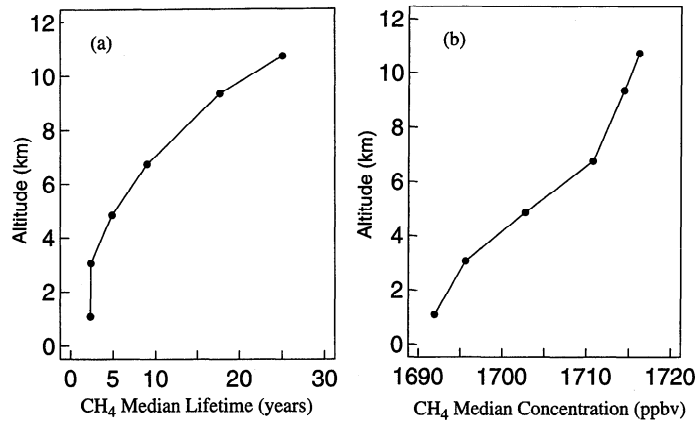

Figure 6. Median CH_4 (a) lifetime and (b) mixing ratio versus altitude.

sions 10, 13, 14, and 15 (M10, M13, M14, and M15). We use measured NO mixing ratios and calculate NO_2 mixing ratios using a point model (see *Jacob et al.*, [1996] for model details) to obtain NO_x values. In the fresh emissions of M10 (Plate 2a), PAN is the dominant form of NO_y with a maximum mixing ratio of 4000 pptv, ~25% larger than the 3000 pptv mixing ratio of NO_x and 4 times greater than the 1200 pptv mixing ratio of HNO_3. The dominance of PAN as an immediate product of NO_x oxidation here contrasts with fossil fuel combustion where HNO_3 usually accounts for a larger fraction of NO_y [*Parrish et al.*, 1993]. After 2 days of aging at 4 km, in M13 (Plate 2b) maximum PAN mixing ratios of 1500 pptv are 3 times the 500 pptv mixing ratio of HNO_3. NO_x mixing ratios have dropped to ~100 pptv which are maintained in the plume in M14 and M15 as the plume ages. After 3 days, in M14 (Plate 2c), HNO_3 has become the dominant form of NO_y at 1000 pptv and maximum mixing ratios of PAN have decreased to 700 pptv. After 5 days, in M15 (Plate 2d), HNO_3 mixing ratios are 600 pptv, and PAN has decreased to 220 pptv. The data thus indicate rapid conversion of emitted NO_x to PAN followed by relatively slow conversion of PAN to NO_x and on to HNO_3 as the plume ages. The effect of rapid PAN formation followed by slow decomposition is to increase the effective lifetime of NO_x, thus helping sustain photochemistry in the plume as it ages. The decrease in total NO_y in the plume as it ages is a result of dilution.

3.2. Modeling

A lagrangian plume model is used to simulate the chemical evolution of this African plume. The model is initialized with mixing ratios determined from the fresh plume sampled during mission 10 at 4 -km altitude and ~11°S latitude and 30°E longitude. The model uses the chemical mechanism described by *Jacob et al.* [1996] to simulate the chemical evolution of the plume over 1 week at 4 -km altitude. Photolysis rates are enhanced by 50% over clear-sky conditions, as indicated by observations, because of persistent stratus cover over the ocean. The ozone column is 7.6×10^{18} molecules cm^{-2}, the mean of values observed above the plume during missions 13, 14, and 15. Initial conditions and background air composition assumed for the calculation are given in Table 5.

Simulations both with and without horizontal plume dilution are conducted. Although the diluting case is more realistic, we use the nondiluting case to examine photochemical influences isolated from the influence of dilution. The width $Y(t)$ of the diluting plume at time t is computed following *Sillman et al.* [1990]:

$$Y(t) = [Y^2 + 8K_y t]^{1/2} \quad (1)$$

where $Y(0)$ is the width of the fresh fire plume assumed to be pumped to 4 -km altitude at time $t = 0$, and K_y is a constant cross-flow diffusion coefficient. We assume $Y(0) = 100$ km, based on AVHRR data for areal extent of fires. In the diluting plume scenario, we choose $K_y = 5 \times 10^4$ m^2 s^{-1} to match the observed decrease of CO_2. This value of K_y is consistent

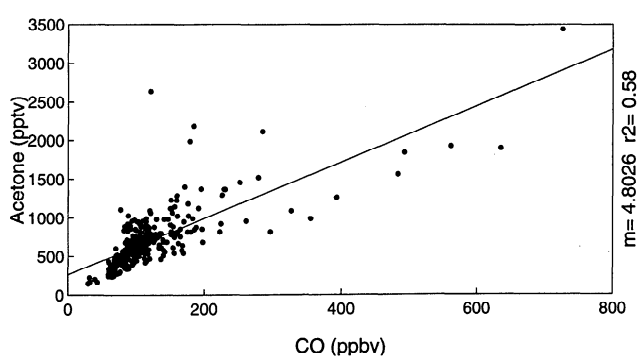

Figure 7. Plot of acetone versus CO for the entire TRACE A data set south of the equator. A positive correlation indicates a regional source of acetone from biomass burning.

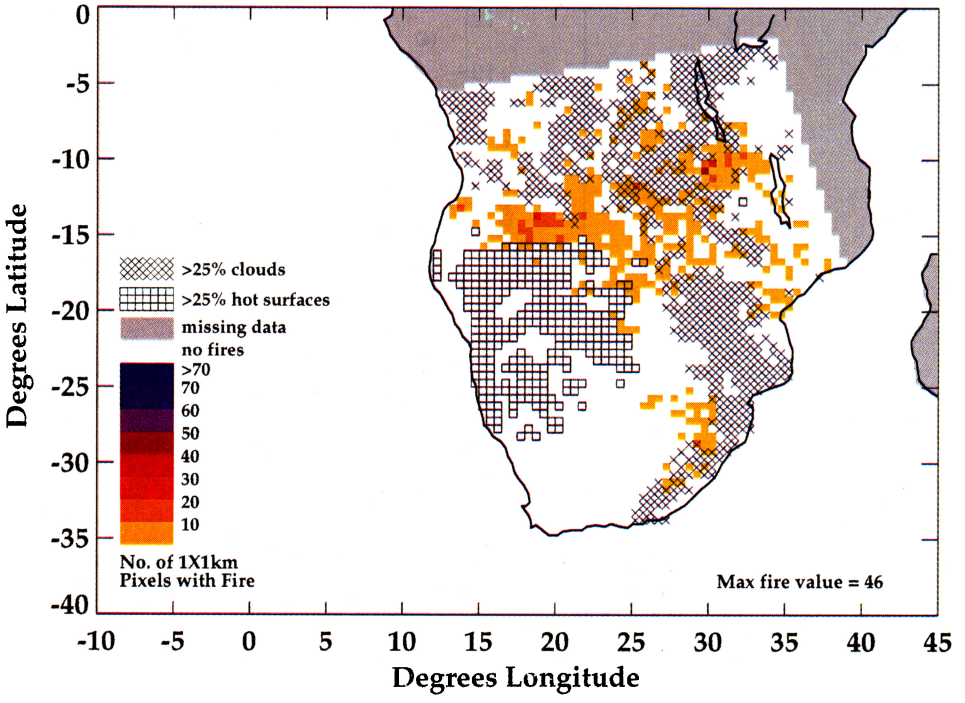

Plate 1. Advanced very high resolution radiometer (AVHRR) remote sensing data showing fire locations on October 12, 1992, the day that back trajectories indicate air parcels intercepted by the aircraft in the plume sampled in flights 13, 14, and 15 were last impacted by biomass burning emissions.

with values recommended by *Gifford* [1982] for plume widening calculations. Concentrations in the diluting plume (C_p) are calculated as mixing ratios and are updated at hourly time steps [t_n, t_{n+1}], by entrainment of background air (C_b) as shown in equations (2) and (3).

$$C_p(t_{n+1}) = C_p(t_n)(1 - \Delta Y) + C_b(\Delta Y) \quad (2)$$

$$\Delta Y = \frac{Y(t_{n+1}) - Y(t_n)}{Y(t_{n+1})} \quad (3)$$

Time-dependent results for the diluting and nondiluting plume simulations are shown in Figure 9 together with the mean plume measurements from missions 10, 13, 14, and 15 superimposed at the appropriate time intervals. The diluting simulation reproduces well the observed mixing ratios for CO and C_2H_2, but the nondiluting simulation shows a 35% decrease of CO over the course of the week due to chemical loss. We see that over the times of plume transport, CO is not a conserved tracer.

The nondiluting plume simulation indicates that 80% of net ozone production occurs within the first 24 -hours of emission. In subsequent days, ozone production is only sufficient to maintain elevated O_3 mixing ratios in the nondiluting plume while the diluting plume experiences net loss. Measurements within the plume on flights 13 and 14 show even lower ozone mixing ratios than are obtained in the diluting plume simulation. The low O_3 production in this plume contrasts with the more generally observed increase of $\Delta O_3/\Delta CO$ from the fresh to the old plume categories (Table 3a). We attribute the discrepancy to the relatively low altitude of the simulated plume, resulting in short lifetimes for both NO_x and O_3.

Photochemical production of ozone in the plume is NO_x-limited as shown in Figure 10. Doubling initial NO, NO_2, HNO_3, and PAN concentrations increased O_3 mixing ratios by ~7 ppbv, while doubling CO, CH_4, and NMHC concentrations increased O_3 mixing ratios by only 2 ppbv throughout the weeklong simulation.

Simulated and observed concentrations of CH_2O and peroxides offer an additional measure of chemical activity in the plume. The initially high mixing ratio of CH_2O indicates that it is primarily emitted during the combustion process or formed rapidly in the fresh plume. Oxidation of propene and ethene helps maintain CH_2O concentrations for the first day. In this simulation, CH_2O has a lifetime of ~4 hours, indicating that net photochemical production, primarily from the oxidation of CH_4, maintains the 400 pptv enhancement above background for the rest of the weeklong simulation.

The diluting and nondiluting model simulations bracket the H_2O_2 measurements, but the model greatly underestimates observed CH_3OOH. The reason for this is unclear but may be due to too low a rate constant in the model for HO_2+CH_3O_2. Model lifetimes of H_2O_2 and CH_3OOH in the simulation are ~0.8 and 0.3 days, respectively, indicating that net photochemical production is responsible for maintaining H_2O_2 mixing ratios above background. Mean $\Delta H_2O_2/\Delta CO$ and $\Delta CH_3OOH/\Delta CO$ enhancement ratios in the data indicate the formation of peroxides as the plumes age; however, in the model this is only observed for H_2O_2 in the nondiluting simulation.

Acetone has a lifetime in the model of ~7 days with losses

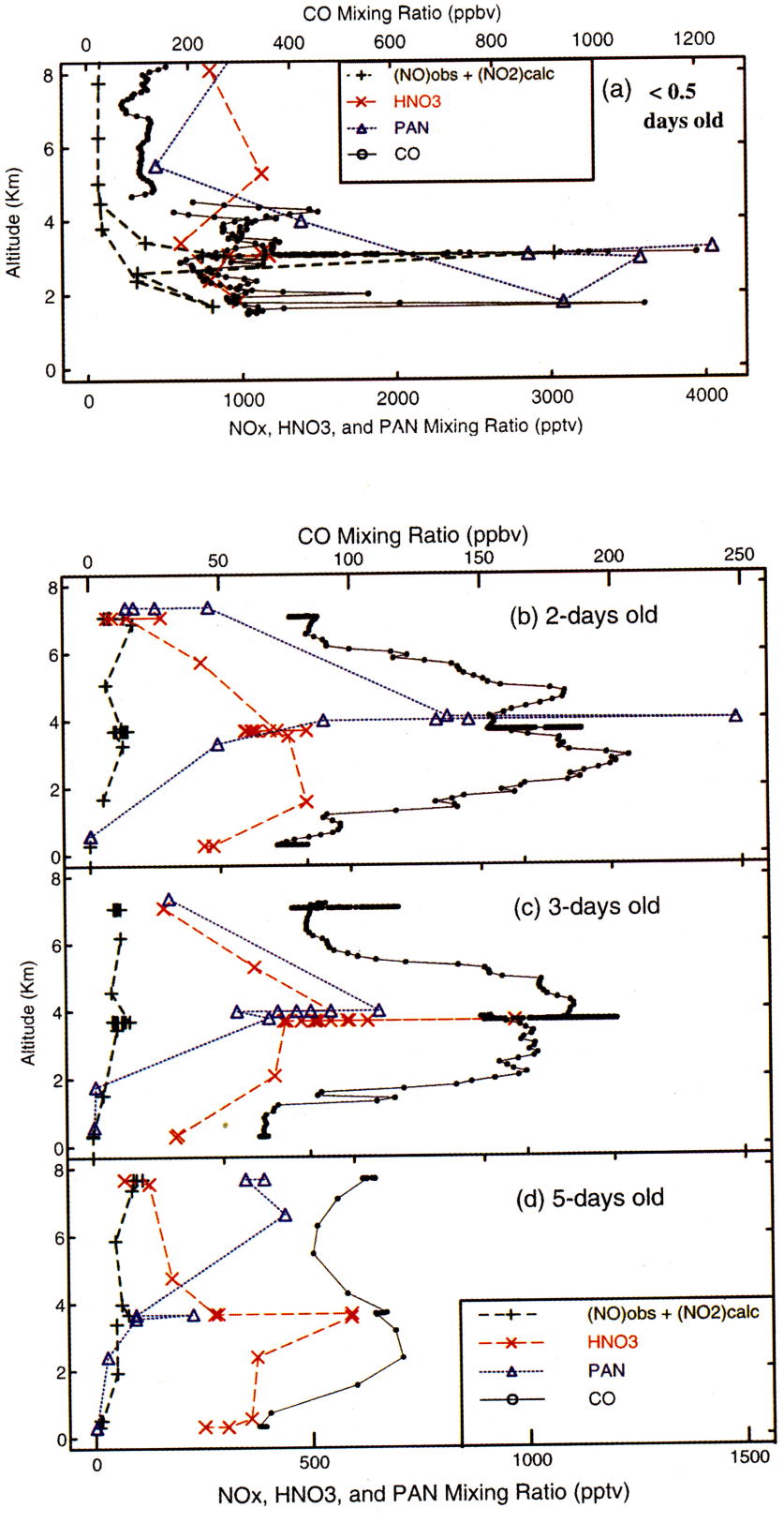

Plate 2. Evolution of NO_y partitioning between NO_x, HNO_3, and PAN. (a) mission 10 measurements of fresh emissions after convection to 4 -km altitude, (b) mission 13 measurements, 2 days, (c) mission 14, 3 days, and (d) mission 15, 5 days after last encountering fresh emissions.

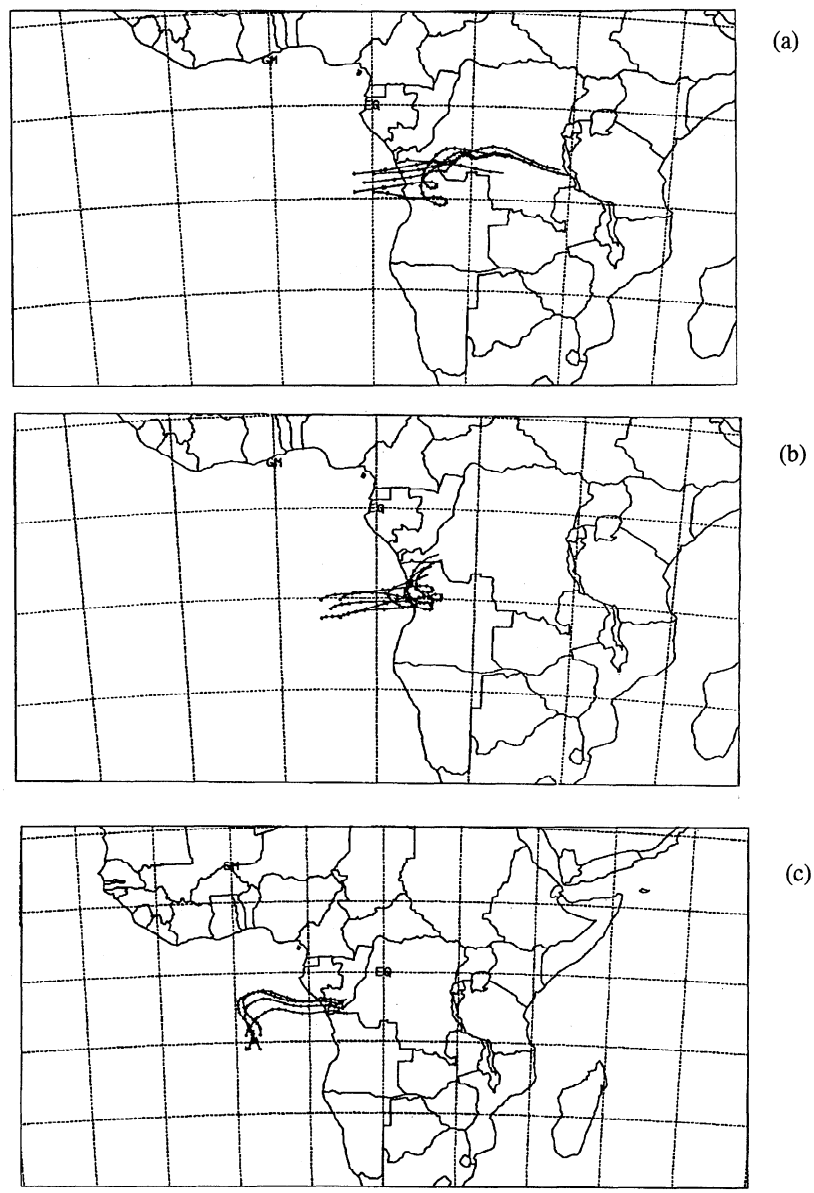

Figure 8. Five-day isentropic back trajectory calculations (Θ = 320 K) for the center of the large biomass burning plume intercepted during (a) flight 13, October 14, 1992, (b) flight 14, October 15, 1992, and (c) flight 15, October 18, 1992 [*S. Bachmeier*, personal communication, 1996]. The back trajectory calculations indicated that the plume remained at approximately 4 -km during transit. Flight 14 was designed to sample the plume 1 day downwind of flight 13. Flight 15 sampled the same plume again 3 days after flight 14.

due to photolysis and reaction with OH. The nondiluting simulation indicates that there is a net photochemical loss of acetone over the week. The model indicates that production which does occur is the result of oxidation of propane and larger NMHC.

The model simulation reproduces well the evolution of NO_y partitioning from domination by PAN in the fresh plume to domination by HNO_3 in the aged plume (see Figure 9). Loss of PAN is primarily via thermal decomposition. Measurements within the plume indicate lower mixing ratios of HNO_3 than our diluting simulation suggests. One possible explanation would be conversion of HNO_3 into nitrate aerosols which is a process not included in the model and which would result in lower HNO_3 concentrations.

4. Regional Budget Analyses

4.1. Scaling Up From Measurements

To examine the relative importance of plumes on regional O_3 production, we plot a cumulative sum of both gross ozone production and loss calculated using the 0-D model versus the CO mixing ratio. Because chemistry varies with altitude, Figure 11 shows these plots in altitude intervals of 8-12, 4-8, and 0-4 km. The cumulative O_3 production at a particular CO concentration represents the total O_3 production which has been cumulatively produced by all points below that CO level. We consider O_3 production occurring in air masses with CO above median mixing ratios to represent O_3 production in plumes. Figure 11 shows that at median

Table 5. Initial Model Conditions for Biomass Burning Plume Simulation

Species	Unit	Initial Concentrations (Fresh Plume)	Background Concentrations[a] (Diluting Plume)
CO_2	ppmv	361	356
CO	ppbv	390	102
O_3	ppbv	85	60
NO	pptv	179	19
NO_2 (calc)	pptv	434	46
HNO_3	pptv	931	277
PAN	pptv	2990	95
CH_4	ppbv	1720	1688
Ethane	pptv	1766	462
Ethene	pptv	1336	5
Acetylene	pptv	1140	80
Propane	pptv	246	17
Propene	pptv	139	2
Butene	pptv	10	0
Benzene	pptv	319	13
Toluene	pptv	98	0
Xylene	pptv	11	0
4C alkanes	pptv	61	0
7C alkanes	pptv	11	0
Isoprene	pptv	38	0
CH_2O	pptv	1580	113
Acetone	pptv	1820	515
Ethanol	pptv	254	0
H_2O_2	pptv	5060	3160
CH_3OOH	pptv	1320	1160
HCOOH	pptv	5130	720

[a] Mixing ratios of background air are taken to be the bottom decile of data sampled between 1and 7 km during portions of flights 13-15 that are in proximity to the plume.

CO in all altitude intervals, not more than 30% of the cumulative gross O_3 production has taken place. The majority of O_3 production takes place in air above the median CO concentration, indicating the importance of the contribution of biomass burning plumes to the regional O_3 enhancement. In contrast, at northern high latitudes, *Mauzerall et al.* [1996] found that biomass burning plumes made a negligible contribution to the region's O_3 budget. Since in the TRACE A region the majority of O_3 production takes place in plumes, we are justified in scaling up from the observed $\Delta O_3/\Delta CO$ enhancement ratio in old plumes (section 2.4) to estimate a minimum regional O_3 production.

To assess the role of biomass burning plumes as regional sources of O_3 for the TRACE A conditions, we scale our enhancement ratio for old plumes ($\Delta O_3/\Delta CO$) as follows:

$$S_{O_3} = \left(\frac{B \cdot E}{A}\right)\left(\frac{\Delta O_3}{\Delta CO}\right)_{old} \quad (4)$$

Here S_{O3} is the net O_3 source from production in biomass burning plumes. B = 294 Tg month^{-1}(Tg = x10^{12}g) is the amount of biomass burned south of the equator in South America and Africa in the month preceding the rainy season [*Hao and Liu,* 1994]. E = 58g CO per 1kg fuel is a CO emission factor for cerrado (grassland) in Brazil [*Ward et al.,* 1992]. $A = 4.8 \times 10^{17}$ cm^2 is the surface area of the South Atlantic air basin (between 65°W and 40°E longitude and 0°S and 40°S latitude) and is used to approximate the region influenced by biomass burning. $(\Delta O_3/\Delta CO)_{old}$ = 0.59 mol mol^{-1} is the mean enhancement ratio observed in old plumes, corrected for an estimated 20% loss of CO. We thus calculate $S_{O3} = 17 \times 10^{10}$ molecules O_3 cm^{-2} s^{-1}.

The average enhancement in the tropospheric O_3 residual (calculated using total ozone mapping spectrometer (TOMS) version 6) from the wet to the dry season in the south Atlantic air basin is ~10 DU (1 DU = 2.69×10^{16} molecules O_3 cm^{-2}) [*Olson et al.*, 1996]. Therefore, with an average residence time of 2-3 weeks in the air basin, the observed tropospheric O_3 enhancement can be generated from O_3 production in biomass burning plumes.

4.2. Model Characterization of Ozone Production in Plumes

In this section we use a point (0-D) photochemical model to evaluate the importance of biomass burning plumes of different ages to the regional O_3 budget. The model is used to calculate diel steady state production and loss rates for O_3 at each point for which measurements exist along the aircraft flight tracks and is described in detail by *Jacob et al.* [1996]. Diel steady state is defined by the reproducibility of concentrations over a 24 -hour solar cycle. CO mixing ratios for each point are used as a proxy for plume age.

The ensemble of aircraft measurements at each point along the flight tracks is merged over the sampling interval of NO for analysis of O_3 production and loss. We divide the points into three altitude ranges (0-4, 4-8, and 8-12 km), and within each altitude range we divide the points based on their observed CO mixing ratio (<70, 70-100, 100-200, 200-300, and >300ppbv). We use the mean CO mixing ratio to indicate the relative time since the parcel was last exposed to biomass burning emissions with CO > 300 ppbv indicating relatively fresh biomass burning plumes, CO between 200-300 and 100-200 ppbv indicating progressively aging

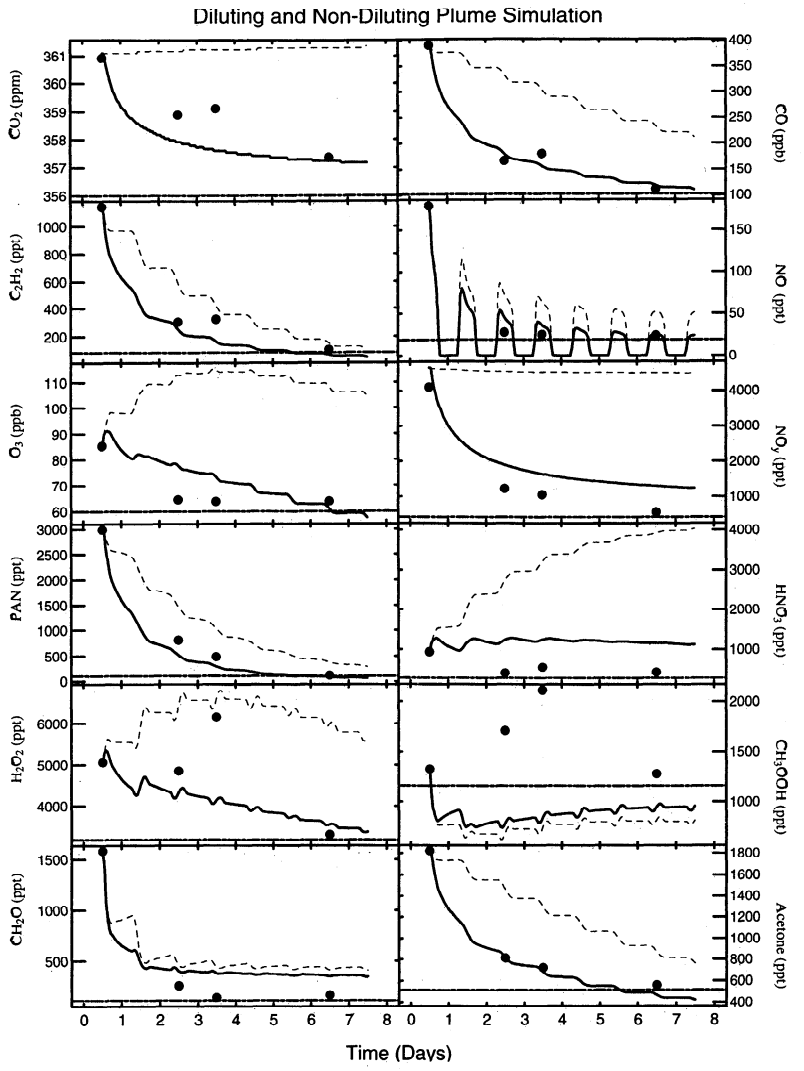

Figure 9. Time-dependent photochemical model simulation at 4 -km. Calculations were started at noon of day 1. Ticks on the x -axis mark midnight. In each panel the thick (thin) solid (dashed) line indicates the evolution of mixing ratios of species in the diluting (undiluting) plume simulation. The thick dashed line indicates the background mixing ratio used to dilute the plume. Points at noon of days 1, 3, 4, and 6 are mean mixing ratios measured within the plume during flights 10, 13, 14, and 15.

biomass burning influence, CO between 70-100 ppbv indicating background air, and CO < 70 ppbv indicating marine boundary layer air in the 0-4 km altitude plot and stratospheric air in the 8-12 km plot. For each altitude range in Figure 12 we plot the mean production and loss rates for O_3 versus the mean CO mixing ratio within each CO interval. Vertical bars on the plots indicate a standard error ($\sigma/\sqrt{n}$) in the mean rates calculated from all points within a particular CO bin.

Figure 12 shows a maximum in gross ozone production and loss at low altitudes and within fresh plumes and shows a decrease in both production and loss as altitude increases and plumes age. O_3 production is dominated by HO_2 + NO with CH_3O_2 + NO being a relatively minor secondary source at all altitudes. O_3 production is largest in the freshest most polluted plumes because of elevated NO_x mixing ratios. In background air at high altitudes, net ozone production remains positive, while in background air at low altitudes, net production is close to zero. In the stratospheric air (mean CO~70 ppbv in the 8-12 km plot) net ozone production remains slightly positive, while in the marine boundary layer (mean CO ~ 70ppbv in the 0-4 km plot), net ozone production is negative. Throughout the column O^1D + H_2O is the primary loss route for O_3, followed by O_3 + HO_2 and O_3 + OH.

We compare the magnitude of ozone production and loss in background air in the wet and dry seasons by conducting a wet season simulation based on a simplified atmosphere including only CO, CH_4, O_3, NO, and H_2O. In order to be a sensitivity analysis of the impact of biomass burning emissions on regional photochemistry, wet season temperatures, dew points, and zenith and nadir UV fluxes were taken from median TRACE A measurements for each altitude interval [*Jacob et al.*, 1996]. Values used in the wet season calcula-

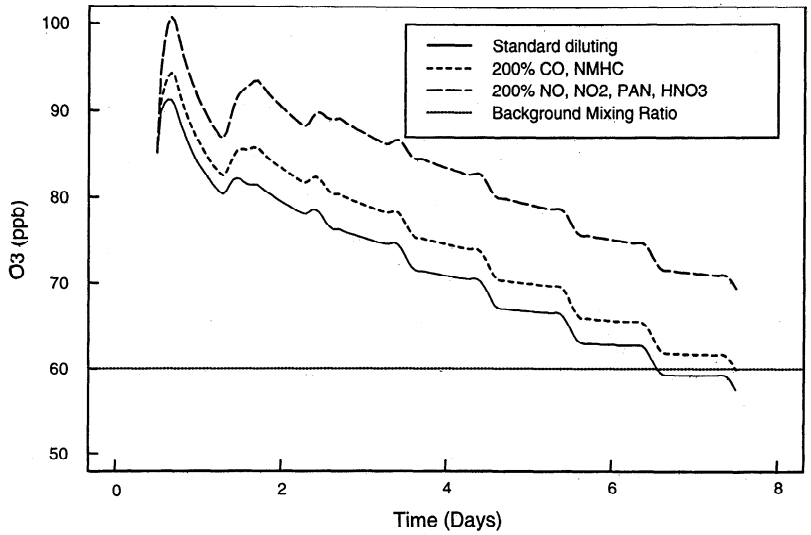

Figure 10. Sensitivity analysis to NO_x versus hydrocarbon limitation on O_3 production in the diluting plume simulation.

tion, and for comparison, median dry season values are shown in Table 6. According to our simulation shown in Figure 12, gross O_3 production in background air during the dry season (70<CO<100 ppbv) is ~3 times larger than gross O_3 production in background air during the wet season (80 ppbv CO). At NO_x mixing ratios below 500 pptv O_3 production is generally limited by the availability of NO_x [*Sillman et al.*, 1990]. Hence, during the dry season we attribute the increased O_3 production to elevation of the NO_x mixing ratio.

5. Conclusions

Photochemistry occurring in biomass burning plumes over the tropical south Atlantic was analyzed using data collected during the TRACE A aircraft expedition conducted during the tropical dry season in September 1992. During TRACE A the chemical composition of biomass burning emissions over source regions and over the South Atlantic were measured. We report enhancement ratios ($\Delta Y/\Delta X$,

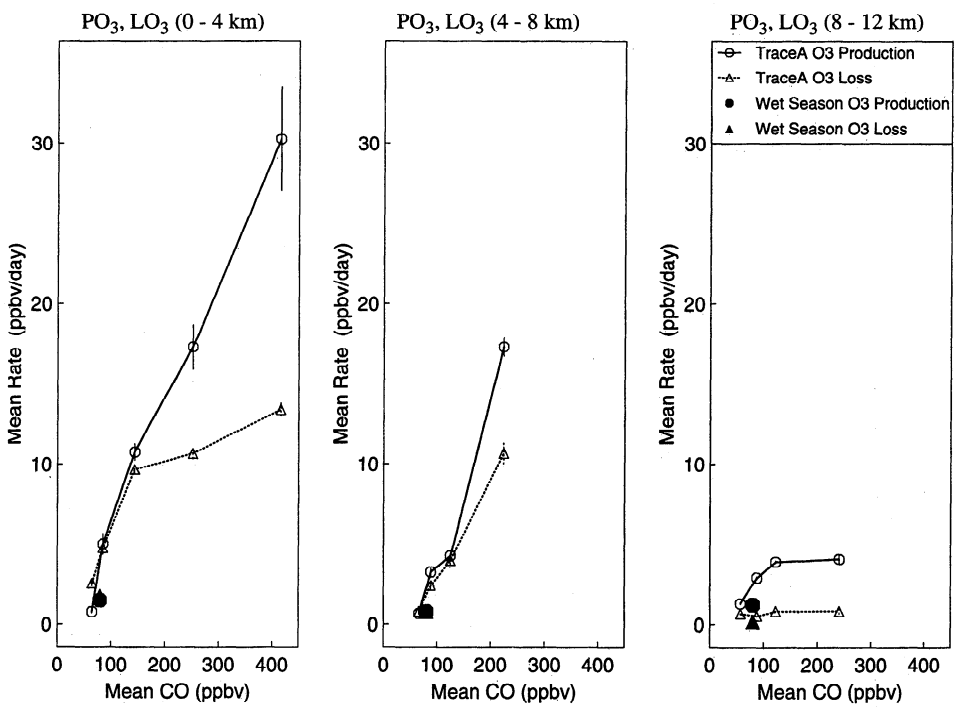

Figure 11. Cumulative sum of O_3 production and loss rates versus CO concentration in altitude intervals 8-12, 4-8, and 0-4 km. O_3 production and loss rates were calculated using a point photochemical model for all TRACE A measurements made south of the equator. The plot shows that the majority of O_3 production occurs at CO mixing ratios above the median, indicating that most O_3 production occurs in plumes.

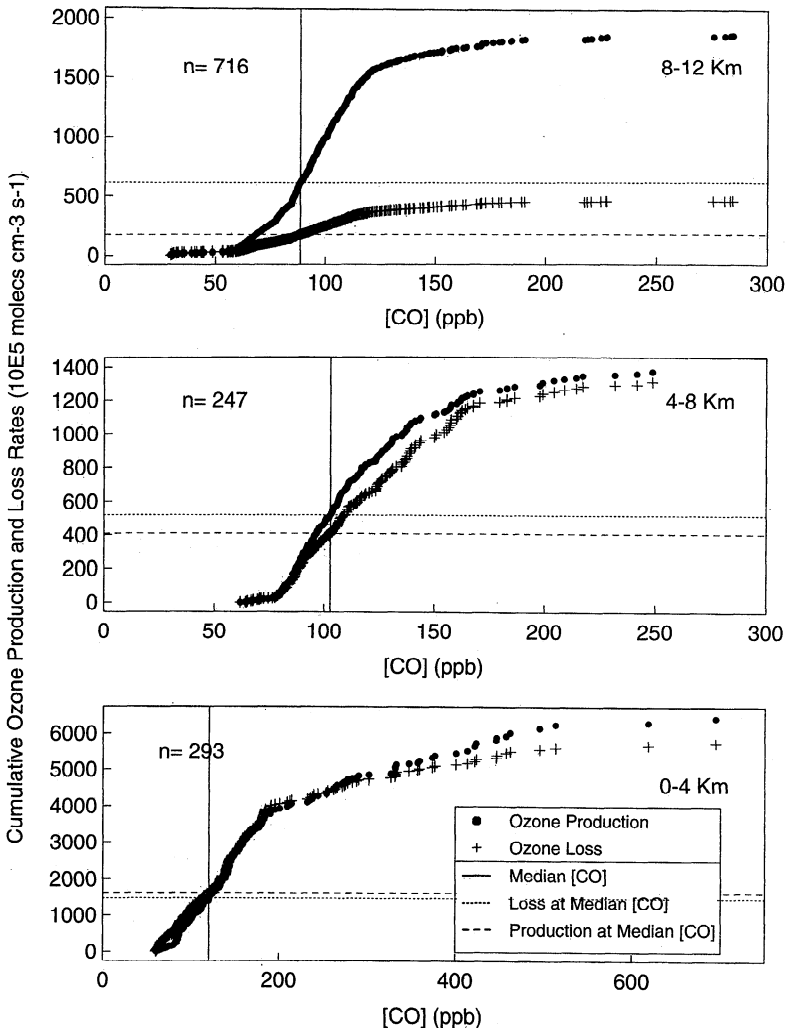

Figure 12. Ozone production and loss versus CO for TRACE A measurements and for simulated wet season points at three altitude intervals (0-4, 4-8, and 8-12 km). Vertical lines represent the standard error on the mean.

where Δ indicates the enhancement of a compound in the plume above the local background mixing ratio, Y is individual NMHC, CO, O_3, CH_4, N_2O, HNO_3, PAN, CH_2O, acetone, H_2O_2, CH_3OOH, HCOOH, CH_3COOH, or aerosols and X is CO or CO_2) as a function of plume age inferred from the progression of ΔNMHC/ΔCO enhancement ratios. We diagnose emission, formation, and loss of species in plumes from progression of enhancement ratios from fresh to old plumes. We find that O_3 is produced in plumes over at least a 1 week period with mean $\Delta O_3/\Delta CO = 0.7$ observed in old plumes; that CH_2O is primarily emitted during the fire or formed shortly thereafter, then subsequently lost as the plume ages; and that acetone is formed after emission as the plume ages. We found $\Delta CO/\Delta CO_2$ decreases from 0.05 to 0.02 from regions of fresh fires to remote ocean locations as a result of the photochemical loss of CO and decreasing background mixing ratios of CO and CO_2. We estimate that a downward correction of ~20% in enhancement ratios relative to ΔCO is necessary in old plumes due to photochemical loss of CO.

In our case study of a large biomass burning plume sampled at 4 -km altitude over the course of 5 days off the west coast of Africa we found elevated concentrations of PAN in the fresh plume. The degradation of PAN helped maintain NO_x mixing ratios in the plume where, over the course of a week, PAN was converted to HNO_3. Ozone production in the plume was limited by the availability of NO_x, and because of the short lifetime of O_3 at 4 -km, net ozone production in the plume was negligible.

We examined the influence that biomass burning plumes have on regional ozone production. We found that the majority of O_3 production takes place in air above the median CO concentration, indicating that most O_3 production occurs in plumes. Maximum gross ozone production and loss rates occur at low altitudes and within fresh plumes. Rates decrease as altitude increases and as plumes age. A simple wet season model simulation indicates that gross O_3 production rates in background air during the dry season are ~3 times larger than during the wet season.

Scaling up from the mean observed $\Delta O_3/\Delta CO$ in old

Table 6. Wet and Dry Season Mixing Ratios

	0-4 km	4-8 km	8-12 km
Wet Season, Values Used in Simulation			
CO[a], ppbv	80	80	80
O_3[b], ppbv	15	30	30
NO[c], pptv	8	8	40
Dry Season, Median TRACE A Mixing Ratios			
CO, ppbv	112	103	93
O_3, ppbv	50	69	74
NO, pptv	25	29	120

[a] CO is assumed to be well mixed throughout the troposphere during the wet season. Mixing ratios are specified from measurements made during the wet season in the lower troposphere over the southern tropical Atlantic Ocean [*Harriss et al.*, 1990].

[b] O_3 values are from wet season ozone sonde measurements made over Amazonia [*Kirchhoff et al.*, 1990].

[c] The 0-8 km mixing ratios are specified from observations during the wet season from *Singh et al.*, [1990]. The 8-12 km mixing ratios are specified from median mixing ratios observed during the wet season on the southern hemispheric portion of flights between Rio de Janeiro and Natal Brazil and between Natal and Dakar, Senegal [*Drummond et al*, 1988].

plumes using a biomass burning emission inventory for CO, we estimate a minimum regional O_3 production of 17 x 10^{10}molecules O_3 $cm^{-2}s^{-1}$. The observed regional enhancement in tropospheric O_3 of ~10 DU from the wet to the dry season [*Olson*, 1996], can be generated from photochemistry in plumes given an average plume residence time in the air basin of 2-3 weeks. Photochemical production of O_3 from biomass burning emissions thus appears able to fully explain the observed 30% enhancement in tropospheric O_3 over the tropical South Atlantic during the dry season. Export of O_3 from this region to the cleaner troposphere above the Pacific Ocean is likely.

Acknowledgments: We thank G. Gardner for compiling the merged TRACE A data sets. This work was supported by NASA Global Tropospheric Chemistry Program and by a NASA graduate student fellowship in global change research to D. L. Mauzerall.

References

Andreae, M. O., et al., Biomass-burning emission and associated haze layers over Amazonia, *J. Geophys. Res., 93*, 1509-1527, 1988.

Andreae, M. O., B. E. Anderson, D. R. Blake, J. D. Bradshaw, J. E. Collins, G. L. Gregory, G. W. Sachse, and M. C. Shipham, Influence of plumes from biomass burning on atmospheric chemistry over the equatorial and tropical South Atlantic during CITE 3, *J. Geophys. Res., 99*, 12,793-12,808, 1994.

Andreae, M. O., et al., Methyl halide emissions from savanna fires in southern Africa, *J. Geophys. Res., 101*, 23,603-23,614, 1996.

Bartlett, K. B., G. W. Sachse, J. E. Collins Jr., and R. C. Harriss, Methane in the tropical South Atlantic: Sources and distribution during the late dry season, *J. Geophys. Res., 101*, 24139-24150, 1996.

Blake, D. R., T. W. Smith Jr., T. -Y. Chen, W. J. Whipple, and F. S. Rowland, Effects of biomass burning on summertime nonmethane hydrocarbon concentrations in the Canadian wetlands, *J. Geophys. Res., 99*, 1699-1720, 1994.

Blake, N. J., D. R. Blake, B. C. Sive, T. -Y. Chen, F. S. Rowland, J. E. Collins Jr., G. W. Sachse, and B. E. Anderson, Biomass burning emissions and vertical distribution of atmospheric methyl halides and other reduced carbon gases in the south Atlantic region, *J. Geophys. Res., 101*, 24,151-24,164, 1996.

Bonsang, B., G. Lambert, and C. C. Boissard, Light hydrocarbon emissions from African savanna burning, in *Global Biomass Burning: Atmospheric, Climatic and Biospheric Implications*, edited by J. S. Levine, pp. 155-161, MIT Press, Cambridge, Mass., 1991.

Bonsang, B., C. Boissard, M. F. Le Cloarec, J. Rudolph, and J. P. Lacaux, Methane, carbon monoxide, and light nonmethane hydrocarbon emissions from African savanna burning during the FOS/DECAFE experiment, *J. Atmos. Chem., 22*, 149-162, 1995.

Browell, E. V., et al., Ozone and aerosol distributions and air mass characteristics over the South Atlantic Basin during the burning season, *J. Geophys. Res., 101*, 24,043-24,068, 1996.

Cahoon, D. R., B. J. Stocks, J. S. Levine, W. R. Cofer, and K. P. O'Neill, Seasonal distribution of African savanna fires, *Nature, 359*, 812-815, 1992.

Chatfield, R. B., J. A. Vastano, H. B. Singh, and G. Sachse, A general model of how fire emissions and chemistry produce African/oceanic plumes (O3, CO, PAN, smoke) in TRACE A, *J. Geophys. Res., 101*, 24,279-24,306, 1996.

Cofer, W. R. III, J. S. Levine, D. I. Sebacher, E. L. Winstead, P. J. Riggan, B. J. Stocks, J. A. Brass, V. G. Ambrosia, and P. J. Boston, Trace gas emissions from chaparral and boreal forest fires, *J. Geophys. Res., 94*, 2255-2259, 1989.

Cofer, W. R. III, J. S. Levine, E. L. Winstead, and B. J. Stocks, Gaseous emissions from Canadian boreal forest fires, *Atmos. Environ., Part A, 24*, 1653-1659, 1990.

Cofer, W. R. III, J. S. Levine, E. L. Winstead, D.R. Cahoon, D. I. Sebacher, J. P. Pinto, and B. J. Stocks, Source compositions of trace gases released during African savanna fires, *J. Geophys. Res., 101*, 23,597-23,602, 1996.

Crutzen, P. J., and M. O. Andreae, Biomass burning in the tropics: impact on atmospheric chemistry and biogeochemical cycles, *Science, 250*, 1669-1678, 1990.

Crutzen, P. J., L. E. Heidt, J. P. Krasnec, W. H. Pollock, and W. Seiler, Biomass burning as a source of atmospheric gases CO, H_2, N_2O, NO, CH_3Cl, and COS, *Nature, 282*, 253-256, 1979.

Delmas, R., J. P. Lacaux, J. C. Menaut, L. Abbadie, X. Le Roux, G. Helas, J. Lobert, Nitrogen compound emission from biomass burning in tropical African savanna FOS/DECAFE 1991 experiment (Lamto, Ivory Coast), *J. Atmos. Chem., 22*, 175-193, 1995.

Drummond, J.W., D. H. Ehhalt, A. Volz, Measurements of nitric oxide between 0 and 12 km altitude and 67 N to 60 S latitude obtained during STRATOZ III, *J. Geophys. Res., 93*, 15,831-15,849, 1988.

Fishman, J., C. Watson, J. Larson, and J. Logan, The distribution of tropospheric ozone determined from satellite data, *J. Geophys. Res., 95*, 3599-3617, 1990.

Fishman, J., J. M. Hoell Jr., R. D. Bendura, R. J. McNeal, and V. W. J. H. Kirchhoff, NASA GTE TRACE A Experiment (September-October 1992): Overview, *J. Geophys. Res., 101*, 23,865-23,880, 1996.

Gifford, F.A., Horizontal diffusion in the atmosphere: A Lagrangian-dynamical theory, *Atmos. Environ., 16*, 505-512, 1982.

Greenberg, J.P., P.R. Zimmerman, L. Heidt, and W. Pollock, Hydrocarbon and carbon monoxide emissions from biomass burning in Brazil, *J. Geophys. Res., 89,* 1350-1354, 1984.

Gregory, G.L., H.E. Fuelberg, S. P. Longmore, B. E. Anderson, J. E. Collins, and D. R. Blake, Chemical characteristics of tropospheric air over the tropical South Atlantic Ocean: Relationship to trajectory history, *J. Geophys. Res., 101,* 23,957-23,972, 1996.

Hao, W. M. and M. -H. Liu, Spatial and temporal distribution of tropical biomass burning, *Global Biogeochem. Cycles, 8,* 495-503, 1994.

Hao, W. M., D. E. Ward, G. Olbu, and S. P. Baker, Emissions of CO_2, CO, and hydrocarbons from fires in diverse African savanna ecosystems, *J. Geophys. Res., 101,* 23,577-23,584, 1996.

Harriss, R. C., G. W. Sachse, G. F. Hill, L. O. Wade, and G. L. Gregory, Carbon Monoxide over the Amazon basin during the wet season, *J. Geophys. Res., 95,* 16,927-16,932, 1990.

Hegg, D. A., L. F. Radke, P. V. Hobbs, R. A. Rasmussen, P. J. Riggan, Emissions of some trace gases from biomass fires, *J. Geophys. Res., 95,* 5669-5675, 1990.

Helas, G., et al., Airborne measurements of savanna fire emissions and the regional distribution of pyrogenic pollutants over western Africa, *J. Atmos. Chem., 22,* 217-239, 1995.

Hirsch, R.M., and E.J. Gilroy, Methods of fitting a straight line to data: Examples in water resources, *Water Resour. Bull., 20,* 705-711, 1984.

Hurst, D. F., D. W. Griffith, J. N. Carras, D. J. Williams, and P. J. Fraser, Measurements of trace gases emitted by Australian savanna fires during the 1990 dry season, *J. Atmos. Chem., 18,* 33-56, 1994a.

Hurst, D. F., D. W. Griffith, and G. D. Cook, Trace gas emissions from biomass burning in tropical Australian savannas, *J. Geophys. Res., 99,* 16,441-16,456, 1994b.

Jacob, D.J., et al., The origin of ozone and NO_x in the tropical troposphere: A photochemical analysis of aircraft observations over the South Atlantic Basin, *J. Geophys. Res., 101,* 24235-24250, 1996.

Kirchhoff, V.W.J.H., I.M.O. Silva, and E.V. Browell, Ozone measurements in Amazonia: Dry season versus wet season, *J. Geophys. Res., 95,* 16,913-16,926, 1990.

Krishnamurti, T. N., H. E. Fuelberg, M. C. Sinha, D. Oosterhof, E. L. Bensman, and V. B. Kumar, The meteorological environment of the tropospheric ozone maximum over the tropical South Atlantic Ocean, *J. Geophys. Res., 98,* 10,621-10,641, 1993.

Lacaux, J. P., J. M. Brustet, R. Delmas, J.C. Menaut, L. Abbadie, B. Bonsang, H. Cachier, J. Baudet, M. O. Andreae, and G. Helas, Biomass burning in the tropical savannas of Ivory Coast: an overview of the field experiment fire of savannas (FOS/DECAFE 91), *J. Atmos. Chem., 22,* 195-216, 1995.

Lacaux, J. P., R. Delmas, C. Jambert, and T. A. J. Kuhlbusch, NO_x emissions from African savanna fires, *J. Geophys. Res., 101,* 23,585-23,596, 1996.

Laursen, K. K., P. V. Hobbs, L.F. Radke, and R. A. Rasmussen, Some trace gas emissions from North American biomass fires with an assessment of regional and global fluxes from biomass burning, *J. Geophys. Res., 97,* 20,687-20,701, 1992.

Lavenu, F. Vegetation map of Africa, Scale 1:1,500,000 Inst. de la Carte Intl. de la Vegetation, Univ. Paul Sabatier, Toulouse, France, 1987. (Distributed by FAO Forest Resour. Assess. 1990 Proj., Rome, Italy, 1987).

Lee, M., B.G. Heikes, D.J. Jacob, G. Sachse, and B. Anderson, Hydrogen peroxide, organic hydroperoxide and formaldehyde as primary pollutants from biomass burning, *J. Geophys. Res., 102,* 1301-1310, 1997.

Lindesay, J.A., M. O. Andreae, J. G. Goldammer, G. Harris, H.J. Annegarn, M. Garstang, R.J. Scholes, and B.W. van Wilgen, International geosphere/biosphere programme/international global atmospheric chemistry SAFARI-92 field experiment: Background and overview, *J. Geophys. Res., 101,* 23,521-23,530, 1996.

Lobert, J. M., D. H. Scharffe, W. -M. Hao, T. A. Kuhlbusch, R. Seuwen, P. Warneck, and P. J. Crutzen, Experimental evaluation of biomass burning emissions: Nitrogen and carbon containing compounds, in *Global Biomass Burning: Atmospheric, Climatic and Biospheric Implications*, edited by J. S. Levine, pp. 289-304, MIT Press, Cambridge, Mass., 1991.

Logan, J. A., and V. Kirchhoff, Seasonal variations of tropospheric ozone at Natal, Brazil, *J. Geophys. Res., 91,* 7875-7881, 1986.

Malingreau, J. -P., and C. J. Tucker, Large-scale deforestation in the southeastern Amazon basin of Brazil, *Ambio, 17,* 49-55, 1988.

Mauzerall, D. L., D. J. Jacob, S.-M. Fan, J.D. Bradshaw, G.L. Gregory, G.W. Sachse, and D.R. Blake, Origin of tropospheric ozone at remote high northern latitudes in summer, *J. Geophys. Res., 101,* 4175-4188, 1996.

McKeen, S. A., and S.C. Liu, Hydrocarbon ratios and photochemical history of air masses, *Geophys. Res. Lett., 20,* 2362-2366, 1993.

Olson, J. R., J. Fishman, V. W. J. H. Kirchhoff, D. Nganga, and B. Cros, Analysis of the distribution of ozone over the southern Atlantic region, *J. Geophys. Res., 101,* 24,083-24,093, 1996.

Parrish, D. D., J. S. Holloway, M. Trainer, P. C. Murphy, G. L. Forbes, F. C. Fehsenfeld, Export of North American ozone pollution to the North Atlantic Ocean, *Science, 259,* 1436-1439, 1993.

Pickering, K. E., et al., Convective transport of biomass burning emissions over Brazil during TRACE A, *J. Geophys. Res., 101,* 23,993-24,012, 1996.

Rudolph, J., A. Khedim, R. Koppmann, and B. Bonsang, Field study of the emissions of methyl chloride and other halocarbons from biomass burning in western Africa, *J. Atmos. Chem., 22,* 67-80, 1995.

Sillman, S., J. A. Logan and S. C. Wofsy, The sensitivity of ozone to nitrogen oxides and hydrocarbons in regional ozone episodes, *J. Geophys. Res., 95,* 1837-1851, 1990.

Singh, H. B., D. O'Hara, D. Herlth, W. Sachse, D. R. Blake, J. D. Bradshaw, M. Kanakidou, and P. J. Crutzen, Acetone in the atmosphere: Distribution, sources, and sinks, *J. Geophys. Res., 99,* 1805-1820, 1994.

Singh, H. B., et al., Atmospheric PAN measurements over the Brazilian Amazon basin during the wet season: Relationships with nitrogen oxides and ozone, *J. Geophys. Res., 95,* 16,945-16,954, 1990.

Singh, H. B., et al., Impact of biomass burning emissions on the composition of the South Atlantic troposphere: Reactive nitrogen and ozone, *J. Geophys. Res., 101,* 24,203-24,220, 1996.

Smyth, S. B., et al., Factors influencing the upper free tropospheric distribution of reactive nitrogen over the South Atlantic during the TRACE A experiment, *J. Geophys. Res., 101,* 24,165-24,186, 1996.

Talbot, R. W., et al., Chemical characteristics of continental outflow over the tropical South Atlantic Ocean from Brazil and Africa, *J. Geophys. Res., 101,* 24187-24202, 1996.

Thompson, A. M., K. E. Pickering, D. P. McNamara, M.R. Schoeberl, R. D. Hudson, J. H. Kim, E. V. Browell, V.W.J.H. Kirchhoff, and D. Nganga, Where did tropospheric ozone over southern Africa and the tropical Atlantic come from in October 1992? Insight from TOMS, GTE TRACE A, and SAFARI 1992, *J. Geophys. Res., 101,* 24,251-24,279, 1996.

Ward, D. E., R. A. Susott, J.B. Kauffman, R. E. Babbitt, D. L. Cummings, B. Dias, B. N. Holben, Y. J. Kaufman, R. A. Rasmussen, and A. W. Setzer, Smoke and fire characteristics for

cerrado and deforestation burns in Brazil: BASE-B experiment, *J. Geophys. Res., 97*, 14,601-14,619, 1992.

Ward, D. E., W. M. Hao, R. A. Susott, R. E. Babbitt, R. W. Shea, J. B. Kauffman, and C. O. Justice, Effect of fuel composition on combustion efficiency and emission factors for African savanna ecosystems, *J. Geophys. Res., 101*, 23,569-23,576, 1996.

Wofsy, S.C., et al., Atmospheric chemistry in the arctic and subarctic: Influence of natural fires, industrial emissions, and stratospheric inputs, *J. Geophys. Res., 97*, 16,731-16,746, 1992.

Wofsy, S.C., S.-M. Fan, D. R. Blake, J. D. Bradshaw, S. T. Sandholm, H. B. Singh, G. W. Sachse, R. C. Harriss, Factors influencing atmospheric composition over subarctic North America during summer, *J. Geophys. Res., 99*, 1887-1897, 1994.

Yokelson, R. J., D. W. Griffith, and D. E. Ward, Open-path fourier transform infrared studies of large-scale laboratory biomass fires, *J. Geophys. Res., 101*, 21,067-21,080, 1996.

B. E. Anderson and G. W. Sachse, NASA Langley Research Center, MS401A, Hampton, VA 23665-5225.

D. R. Blake, Department of Chemistry, University of California at Irvine, Irvine, CA 92717.

J. D. Bradshaw, School of Earth and Atmospheric Sciences, Georgia Institute of Technology, Atlanta, GA 30332.

B. Heikes, Graduate School of Oceanography, University of Rhode Island, Narragansett, RI 02882.

D. J. Jacob and J. A. Logan, Department of Earth and Planetary Science and the Division of Applied Science, Harvard University, Cambridge MA 02138.

D. L. Mauzerall, National Center for Atmospheric Research, P. O. Box 3000, Boulder, CO 80307-3000. (e-mail: dlm@ucar.edu)

H. Singh, NASA Ames Research Center, MS2455, Moffett Field, CA 94035.

B. Talbot, Institute for the Study of Earth, Oceans and Space, University of New Hampshire, Durham, NH 03824.

(Received November 22, 1996; revised September 9, 1997; accepted September 10, 1997.)